Surfaces and Interfaces 44 (2024) 103797

Contents lists available at ScienceDirect

Surfaces and Interfaces

journal homepage: www.sciencedirect.com/journal/surfaces-and-interfaces

Effect of electrolyte composition on the formation of PEO coatings on AA2024 aluminium alloy

G. Yeshmanova [a,b], C. Blawert [b], M. Serdechnova [b,*], D.C. Florian Wieland [c], M. Starykevich [d], E. Gazenbiller [b], D. Höche [b], D. Smagulov [a], M.L. Zheludkevich [b,e]

[a] Satbayev University, 22 Satbayev Street, Almaty 050013, Kazakhstan
[b] Institute of Surface Science, Helmholtz-Zentrum Hereon, Max-Planck Strasse 1, Geesthacht 21502, Germany
[c] Institute of Metallic Biomaterials, Helmholtz-Zentrum Hereon, Max-Planck Strasse 1, Geesthacht 21502, Germany
[d] Department of Materials and Ceramic Engineering, CICECO - Aveiro Institute of Materials, University of Aveiro, Aveiro 3810-193, Portugal
[e] Faculty of Engineering, CAU Kiel University, Kaiserstrasse 2, Kiel 24143, Germany

ARTICLE INFO

Keywords:
Plasma electrolytic oxidation (PEO)
AA2024 aluminium alloy
Alkaline electrolytes
Growth mechanisms

ABSTRACT

Since the electrolyte composition plays a crucial role in the plasma electrolytic oxidation (PEO) coating formation process, a systematic and in-depth study was proposed to identify an electrolyte composition for fast PEO coating growth on AA2024 alloy. Different concentration ratios of mixed alkaline electrolytes (hydroxide, silicate and phosphate) were investigated. PEO process was conducted at low constant current density of 50 mA/cm^2, which is intended for lowering the energy consumption. Results demonstrated that the breakdown voltage of PEO coatings is directly proportional to the logarithm of electrolyte resistivity. The coating growth mechanism showed two main directions. The thickening of the coating mainly depends on the rapid deposition of electrolyte compounds in Si-based electrolyte, and the coating growth occurs mainly towards the electrolyte/coating interface. Contrary, in OH-, and P-based electrolytes, the inward coating growth was dominating mainly by substrate oxidation. A variety of phases as a function of different electrolyte compositions and final voltages were observed. With high final voltages (over 470 V) for coatings produced in mixed electrolytes with low concentrations of hydroxide, silicate or phosphate (2 and 6 g/L), γ-Al_2O_3 crystalline phase predominates in the PEO layer composition. However, only a low efficiency of coating growth can be reached. In the electrolytes with high silicate concentrations accompanied by an increase of phosphate concentration, the final voltage is around 455 V and the coating composition is dominated by an amorphous phase in combination with crystalline mullite and γ-Al_2O_3. High silicate-phosphate contents (18–24 g/L) in mixed electrolytes with low final voltages of about 360 V results in a fully amorphous PEO layer and significantly increases coating thickness. A combination of low content of hydroxide, high silicate with increasing content of phosphate in mixed electrolyte increases the coating thickness, and improves the density and uniformity of the overall PEO layers.

1. Introduction

Since decades, plasma electrolytic oxidation (PEO) has been successfully used for surface treatment of different alloys (Al, Mg, Ti, etc.) [1–5]. The process results in a modification of the surface and formation of a protective oxide-based coating. Obtained ceramic coatings have high hardness, strength, good adhesion between substrate and coating and high thermal stability [6–8]. The main constituents of the PEO coatings are high-temperature oxide phases, which are synthesized during the electric discharges, combining substrate and electrolyte species and convey high corrosion, tribological, photocatalytic, biomedical, thermal-barrier and other specific properties [9–13].

Up to now, significant progress has been made to understand the micro-discharge phenomena and the coating growth mechanisms as well as the main factors affecting the formation and properties of oxide coatings during PEO processing on aluminium [14–16]. It was shown that the structure, composition, and properties of PEO layer are closely related to the composition of electrolyte bath [17,18]. The main electrolytes for PEO treatment on Al (Ti, Mg, etc.) are eco-friendly aluminate-, silicate- and phosphate-based alkaline electrolytes [19,20], which

* Corresponding author.
E-mail address: maria.serdechnova@hereon.de (M. Serdechnova).

https://doi.org/10.1016/j.surfin.2023.103797
Received 11 September 2023; Received in revised form 28 November 2023; Accepted 21 December 2023
Available online 22 December 2023

make it easy to achieve discharge voltage and contribute to the coating growth. Obviously, the PEO process leads to high energy consumption due to the significantly high voltage and current applied [21]. Numerous studies focus on reducing the energy consumption during the PEO process and make it economically viable for various applications. The decrease of the discharge voltage by using more concentrated electrolytes [22] and applying bipolar current mode [23,24] are beneficial to achieve high coating growth rate as well as energy efficiency. On the other hand, the oxygen evolution does not require much current, since alumina has very low electron conductivity and the current transfer occurs mainly by ions [21]. Alternative approaches, such as an addition of solid particles [25], hybrid/composite coatings [26], or pre-anodization step [27,28] to improve the effectiveness of PEO coating formation and optimization of intended PEO performance on aluminium have been proposed.

In fact, different coating formation mechanism using alkaline electrolytes on different alloys (Al, Mg, etc.) have been observed during PEO process [29–32]. It was reported that under certain current densities, more energy is required in the phosphate-based electrolyte system in comparison with silicate one resulting in a higher ratio of hard corundum phase (α-Al_2O_3) [20]. With respect to the PEO coating uniformity, it is argued that the silicate-based electrolyte system is more favourable than the phosphate-based one on aluminium substrate, due to the formation of stable PEO coating with more homogeneous morphology [17]. Similarly, PEO process, performed on magnesium substrate using silicate and phosphate electrolytes, resulted in a thicker, more adhesive, homogeneous coating, when performed in silicate electrolyte (~100 μm). This layer also exhibits higher tribocorrosion performance than the one obtained in phosphate electrolyte (~40 μm) [33]. By increasing the silicate content in the electrolyte, the possibilities to form a thick composite Al_2O_3-nSiO_2 PEO coatings on aluminium substrate was also shown [34]. In addition, the phase composition of the coatings can vary due to the participation of silicate ions from the electrolyte in the reactions of coating formation and their incorporation into the coating structure [35]. Recently, PEO coatings formation in phosphate, silicate and aluminate electrolytes on SiCp/Al composites and their characterization have been performed [36]. A significant difference in the plasma discharges is revealed, where the local temperature ranges are approximately 6000–12,000 K for silicate electrolyte, 6000–10,000 K for aluminate electrolyte and 4000–5000 K for phosphate electrolyte. The phase composition of coatings, obtained under high temperature (silicate and aluminate electrolytes) is based on crystalline aluminium oxide and mullite. It results in good wear and corrosion resistance of the substrate. For coatings, formed under lower temperature (in phosphate electrolyte), an amorphous phase was predominant, demonstrating poorer performances of the layers. In another work [37], the microstructure and growth mechanisms of PEO coatings obtained in silicate, phosphate and mixed electrolytes were characterized in detail. The results showed that silicate deposition dominates the growth of the PEO coating in the silicate electrolyte, and the Si element is located throughout the coating. The formation of the coating in the phosphate electrolyte mainly depended on the oxidation of the aluminium matrix, growing inwards towards the substrate. The coating obtained in the mixed electrolyte was similar to one obtained in the phosphate electrolyte: the substrate oxidation predominated, supplemented by the deposition of electrolyte species. The use of the electrolytes with mixed composition resulted in a dense structure (low porosity of PEO layer) and a superior surface quality.

Summarising, there are quite a lot of studies using various electrolyte compositions for PEO processing, however, not much is done under the aspect to optimize coating growth under low current densities conditions. The role of different double and triple (hydroxides, silicates, phosphates) electrolyte concentration ratios on the PEO coating formation on AA2024 alloy is still interesting under the aspect of energy consumption and to improve the PEO coating quality and formation efficiency.

Therefore, this work focuses on the formation of PEO coatings on AA2024 aluminium alloy with fast coating growth rate in spite of low current density (50 mA/cm^2) applied. The modification of oxidation behaviour during PEO processing and coating evolution in a mixed composite electrolyte system (hydroxides, silicates, phosphates) was studied based on morphology, elemental distribution and phase formation.

2. Experimental

Rectangular *samples* of rolled aluminium alloy AA2024 sheet (D16T, according to GOST 4784–97) with sizes of 20 mm × 30 mm × 1.6 mm and nominal composition in wt.%: 3.8–4.9 Cu, 1.2–1.8 Mg, 0.5 Fe, 0.5 Si, 0.3 Zn, 0.3 Mn and Al balance – were selected. Before PEO treatment, the specimens were cleaned with ethanol and dried in air.

PEO processing was perform using a pulsed DC source. A current density of 50 mA/cm^2, under a constant voltage limit of 500 V, a frequency of 200 Hz with a pulse ratio equal to t_{on}: t_{off} = 0.5ms:4.5 ms and a treatment time of 20 min were settled. The oxidation process was carried out in a PVC vessel equipped with a combined cathode/stainless steel coil heat exchanger. Samples connected to a conductive holder were used as the anode. The experiments were conducted in different concentrations of mixed alkaline electrolytes, which were cooled using a water-cooling system to a constant temperature of 20 ± 1 ºC. Respective electrolyte pH (691 pH meter, Metrohm, Germany) and conductivity (SevenMulti, Mettler Toledo) measurements are given in Table 1. For clarity, specimens are grouped in four sets as labelled in Table 1.

During the PEO process, *the oxidation voltage* as a function of the treatment time was recorded, using a data acquisition system SignalSoft 6000 software package (Gantner Instruments, Germany). *The surface morphology and cross-section* of the coatings were studied using Tescan-Vega3SB scanning electron microscope (SEM, Tescan, Czech Republic). Samples for cross-section analysis were mount in an epoxy resin and first ground with SiC abrasive paper (from 500# to 2500#) and then polished using diamond paste (1 μm). *The element distribution/composition* on the surface and cross-section of the coatings was examined by an energy dispersive spectrometer system (eumeX, EDS, Germany) equipped with the SEM. *The surface porosity* as well as the average pore size was measured by analysing SEM images of the surface of the coatings using the image processing software “Image J”, and the surface porosity of PEO coatings was calculated by the ratio of the area occupied by the pores to the total image area (magnification 500 ×). The change in *surface roughness* of the coatings R_a, as the arithmetic mean deviation of the roughness profile, was measured using laser scanning confocal microscope (LSM 800, ZEISS, Germany) (magnification 2000 ×). *The thickness* measurements were carried out using a thickness gauge MiniTest 2100 (Elektro Physik, Germany) and by observing the cross-section in SEM. *The optical cross-section views* of coatings were obtained applying optical microscopy (OLYMPUS BX53M) to analyse the coating growth direction (inwards/outwards). For that purpose, a part of the surface was covered to prevent the coating growth and keep “zero level” interface.

The phase composition of the coatings was determined using X-ray diffraction measurements (XRD, D8 Advance, BrukerAXS) with Ni filtered Cu K_α radiation operated at 40 kV/40 mA. Diffraction patterns were obtained in the 2θ range from 20º to 80º with a step size of 0.02º/s and grazing angle of 3º.

The depth profile analysis of the PEO coatings was performed by glow discharge optical emission spectroscopy (GDOES) (GD-Profiler 2, HORIBA, France), where coupling of radiofrequency-pulsed glow discharges to emitted light detectors enables a quasi-simultaneous extraction of all atoms, consequently, rapid depth profiling of thick coating [38]. A standard 4 mm copper anode with a distance of 0.1 mm from the sample was used. Argon was used as a plasma gas at an operating pressure of 650 Pa and a power of 30 W. No special sample preparation method was used prior to the analysis.

Table 1
PEO specimens, respective electrolyte compositions, pH and conductivity. The colours are added for easier visibility of the selected groups of electrolytes.

Group	Specificity	Specimen	Electrolyte composition			pH	Conductivity
			KOH (g/L)	Na_2SiO_3 (g/L)	Na_3PO_4 (g/L)		
Base electrolytes	OH-based electrolyte	18K2Si2P	18	2	2	13.2	68.8
	Si-based electrolyte	2K18Si2P	2	18	2	12.9	40.7
	P-based electrolyte	2K2Si18P	2	2	18	12.7	27.6
P-based electrolyte	with increasing concentration of hydroxide	**2K**2Si18P	2	2	18	12.7	27.6
		6K2Si18P	6	2	18	12.9	39.5
		18K2Si18P	18	2	18	13.1	74.1
	with increasing concentration of silicate	2K**2Si**18P	2	2	18	12.7	27.6
		2K**6Si**18P	2	6	18	12.8	33.5
		2K**18Si**18P	2	18	18	13.0	48.9
Si-based electrolyte	with increasing concentration of phosphate	2K18Si**2P**	2	18	2	12.9	40.7
		2K18Si**6P**	2	18	6	12.9	42.4
		2K18Si**18P**	2	18	18	13.0	48.9
Mixed electrolyte	with increasing concentration of Si:P	2K**12Si12P**	2	12	12	12.9	37.3
		2K**18Si18P**	2	18	18	13.0	48.9
		2K**24Si24P**	2	24	24	13.0	58.1
	with increasing concentration of OH:Si:P	**2K2Si2P**	2	2	2	12.6	14.4
		6K6Si6P	6	6	6	13.0	37.6
		18K18Si18P	18	18	18	13.3	90.1

The phase composition/distribution across the coating was studied at the synchrotron PETRA III (DESY, Hamburg, Germany) at the nano focus end station of P03 beamline, with an X-ray energy of 19.8 keV and a beam size of 1.5 μm × 1.5 μm [39]. The phases composition of the coating and interface regions were investigated by performing a mapping (mesh) scan [39], with a size of 45 × 45 points with a step size of 2 and 2 μm, in perpendicular and lateral directions, respectively. This resulted in a measured area of 90 × 90 μm. An Eiger 9 M detector (pixel size 75 μm × 75 μm) with an acquisition time of 0.5 s was used. Data reduction was conducted by pyFAI [40]. Analysis of the diffraction data and the two-dimensional analysis was performed by an in house developed Matlab code. The diffraction profiles were normalized to the ionization current in a gas chamber setup in front of the sample along the beam path. That allows to correct X-ray beam intensity variations, making the total scattered intensity directly proportional to the gauge volume. Each two-dimensional map consisted out of 2025 diffraction patterns from which the scattered intensity of distinct X-ray phases was extracted. By plotting this intensity in a two dimensional map, the spatial phase distribution within the layer can be visualized. This script was used to plot 2D maps of the distribution of main phases in the coating.

3. Results

3.1. Voltage–time curves

3.1.1. Voltage evolution for PEO coatings obtained in base electrolytes

The PEO process was operated fully under galvanostatic conditions in all cases. The preselected current density value of 50 mA/cm^2 was not enough to reach the selected voltage limit of 500 V. Fig. 1 shows the voltage-time curves for different PEO coatings prepared in the base electrolytes. The point, at which the first spark discharge occurs, was defined as the breakdown voltage. After the breakdown of the primary oxide layer, a turning point appears in the voltage curve. This corresponds to the formation of numerous small short living plasma discharges [37]. Through the duration of PEO process, voltage increases with the increase of the treatment time, and sparks become more intensive as well.

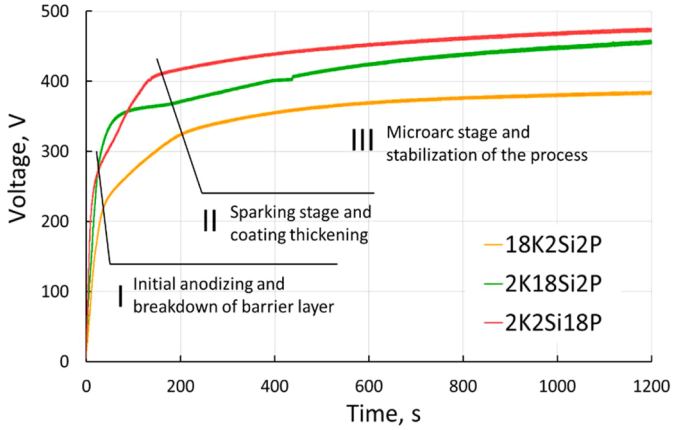

Fig. 1. Voltage-time curves for PEO coatings formed in base electrolytes.

Detailed analysis of the voltage response for coatings obtained in base electrolytes demonstrates three stages, as consistent with previous studies [30,41]. Stage I corresponds to the beginning of the process; voltage increases linearly and sharply within the first 50 s. Then, the dielectric breakdown occurs and numerous white colour small discharges appear. During stage II, voltage rises slower with processing time (lasts from around 50 s till 200 s), that contributes to the increase of the thickness and resistance of the layer. During the last stage III (starting from around 200 s), the voltage steadily increases and discharges become more intense with changing their colour to yellow and then to orange, similarly as it was shown previously [42].

From Fig. 1, it can be seen that the value of breakdown voltage appears earlier in OH-based electrolyte (18K2Si2P) at around 220 V probably due to its high conductivity. The final voltage reaches 385 V. For Si-based electrolyte (2K18Si2P) the highest breakdown voltage of around 280 V is observed, and the final voltage reaches 455 V. In the P-based electrolyte (2K2Si18P) a lower breakdown voltage of 260 V and the highest final voltage of 475 V were registered.

Oppositely going trends in the breakdown (V_B) and final voltages (V_F), reached in P-based (V_B – 260 V, V_F – 475 V) and Si-based electrolytes (V_B – 280 V, V_F – 455 V) can be observed (**Table SI-1**). However, the breakdown voltage dependence from the electrolyte conductivity is not that straightforward for both Si- and P-based groups of electrolytes: in Si-based electrolyte the conductivity is higher (40.7 mS/cm) than that in P-based electrolyte (27.6 mS/cm). In that case, the breakdown voltage can be also affected by the different composition and formation of initial layer, as well as the insulating properties of the barrier oxide layer in respective electrolytes, as discussed in [11]. The difference between the breakdown voltage and the final voltage is a kind of indicator of phase stability at high temperatures and pressures.

3.1.2. *Voltage evolution for PEO coatings obtained in P-based electrolyte system*

In P-based electrolyte system with a gradual increase in hydroxide content (Fig. 2(**a**)), the breakdown and final voltages decrease with a conductivity increase. The intensity of discharges becomes stronger over time as well. The voltage-time slope shows three successive stages as marked in Fig. 2(**a**). Breakdowns of the dielectric barrier layer for specimens 2K2Si18P, 6K2Si18P, 18K2Si18P occurs at 260, 250 and 210 V, respectively. The corresponding final voltages are 475, 455 and 378 V.

With an increase of silicate content, a similar breakdown voltage at around 260 V was registered for the specimens 2K2Si18P and 2K6Si18P (Fig. 2(**b**)). The final reached voltages are 475 and 470 V, respectively. The three stages are determined during the treatments. In 2K18Si18P specimen, the breaking down of initial oxide layer occurs at around 250 V, and after the onset of stage III, the discharge voltage remains relatively low without further increase until the end of the treatment (330 V). The treatment is characterized by discharges with visibly less intensity. This might be explained via the inhomogeneity of the forming coating. After breaking down of the barrier layer, the coating is no longer growing uniformly, forming island-like coating clusters on the top of the surface.

3.1.3. *Voltage evolution for PEO coatings obtained in Si-based electrolyte system*

In Si-based electrolyte system with increasing concentration of phosphate, a similar value of breakdown voltage for the 2K18Si2P,

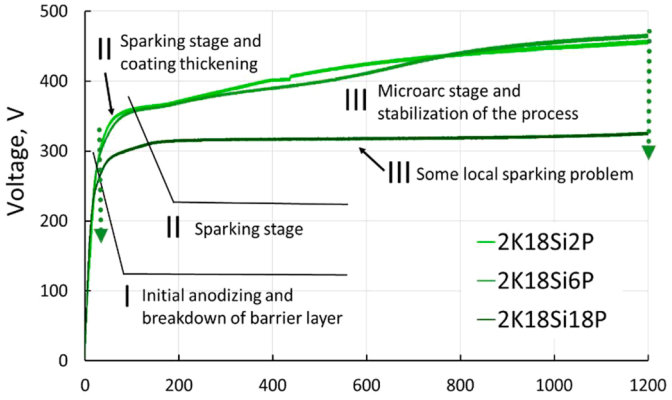

Fig. 3. Voltage-time curves for PEO coatings formed in Si-based electrolyte system with a gradual increase of the phosphate content.

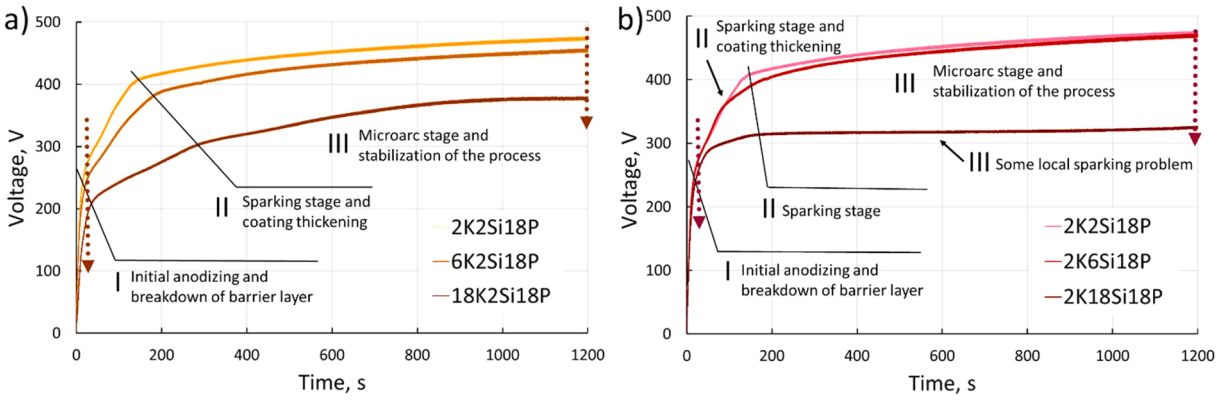

Fig. 2. Voltage-time curves for PEO coatings formed in P-based electrolyte system with a gradual increase of the hydroxide content (a), and with a gradual increase of the silicate content (b).

2K18Si6P specimens at around 280 V is observed (Fig. 3). Corresponding final voltages are 465 V and 466 V, respectively. However, visually more intense discharges were noticed in Si-based electrolyte than in the P-based electrolyte system.

3.1.4. Voltage evolution for PEO coatings obtained in mixed electrolyte system

In the mixed electrolyte group with a gradual increase of both silicate and phosphate concentrations (Fig. 4(a)), two more compositions were added with lower (2K12Si12P) and higher (2K24Si24P) contents of Si- and P-based compounds in the electrolyte to understand more about the behaviour of the treatment in 2K18Si18P electrolyte. The 2K12Si12P treatment has a typical voltage-time curve with three stages, higher breakdown voltage is at around 270 V, and higher final voltage equal to 475 V in this system. The process runs with intensive discharge sparks. Whereas for the 2K24Si24P treatment the curve type is different. After reaching the breakdown voltage of 220 V at stage I, the voltage continues to rise steadily with some fluctuations during the following-up stages. Discharges become more powerful. At ca. 900 s of treatment, the process reaches stage IV with a maximum voltage value of 430 V changing of sparks colour from yellow to orange. Moreover, the many stages (I-IV) may indicate a reluctant coating growth in 2K24Si24P. Afterward, local white stronger discharges appear (plasma arcing) and the voltage drops sharply down from 460 to 400 V (stage V). Local stationary burning on the surface of the specimen is observed by visual inspection at this moment. Then, after ca. 1100 s of treatment time, the voltage stabilizes at 360 V until the end of PEO processing (stage VI).

With increasing equal concentrations of all components (Fig. 4(b)), three stages are observed in the curve. At the lowest concentration of electrolyte (2K2Si2P) the highest breakdown (380 V) and final (499 V) voltages were found. The strong discharge noise was noticed during the process, possibly due to the thin forming layer. With a gradual increase of electrolyte concentrations, the breakdown voltages correspondingly decrease with increase of the electrolyte conductivity. For 6K6Si6P specimen, the less intensity of discharge noise was noticed. The long-lasting large sparks are predominating in the process with increasing the electrolyte concentrations (18K18Si18P). The lowest breakdown voltage at around 200 V was registered and final voltage of 389 V was reached.

In general, it is noted that the chemical composition of the electrolytes and their conductivity influence the breakdown and final voltages during the PEO processing. An increase in conductivity comes with an increase of the concentrations of electrolytes. This influences the breakdown voltage as well as the final processing voltage, which decrease for all P-, Si-based and mixed electrolyte series with concentration increase.

The dependence of breakdown voltage (V_B) from the logarithm of electrolyte resistivity (ρ) for PEO coatings given in Fig. 5. The dependence can be represented by a line that satisfies the empirical equation [43]:

$$V_B = 281\log(\rho) + 173 \quad (1)$$

Some deviation points can be attributed either to the oxidation process or to the structure defects of the oxide layer.

3.2. Surface morphology and chemical composition

3.2.1. Surface morphology for PEO coatings obtained in base electrolytes

Fig. 6 shows the surface and cross-sectional morphologies of PEO coatings fabricated in base electrolytes. The surface morphologies of the coatings are dominated mostly by crater- and volcano-like structures with numerous pores and cracks. This observation is in good agreement with previously published results [1,11,25]. The surface features overall can be characterized by pore distribution, which are mainly created by the discharge channels due to the rapid solidification of the melting coating materials and gas evolution. The surface porosity, number of pores and the surface roughness (R_a) for all the produced coatings are given in **Table SI-2.**

For the specimen obtained in OH-based electrolyte (18K2Si2P) (Fig. 6(**a**)), a large size open pores (14.0 ± 1.3 μm) surrounded by molten species in volcano-like forms is observed, giving an overall surface porosity of 15.4 ± 1.5% (number of pores is 1963 ± 319). However, the coating surface demonstrates relatively low roughness, being produced in OH-based electrolyte (1.5 ± 0.3 μm) as well as in P-based electrolyte (1.4 ± 0.1 μm) in comparison with silicate-based electrolyte. PEO processing in Si-based electrolyte (2K18Si2P) (Fig. 6(**b**)) resulted in

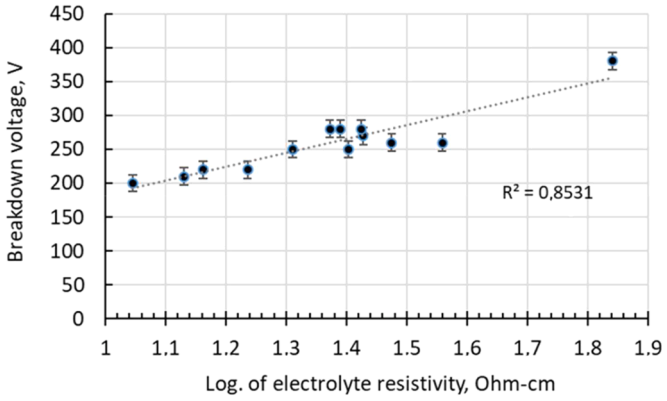

Fig. 5. Breakdown voltage as a function of the logarithm of electrolyte resistivity for different PEO coatings.

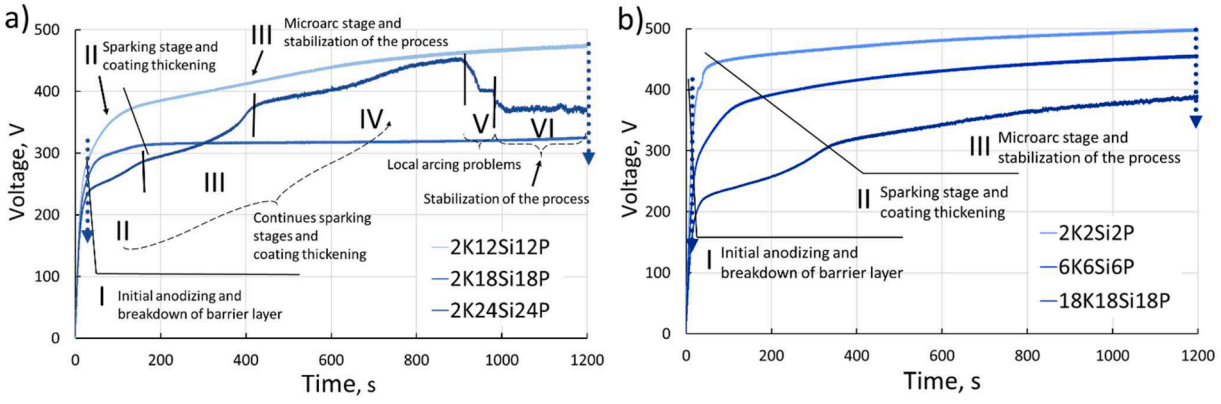

Fig. 4. Voltage-time curves for different PEO coatings formed in mixed electrolyte system: equally increasing contents of silicate and phosphate (a), and equally increasing contents of hydroxide, silicate and phosphate (b).

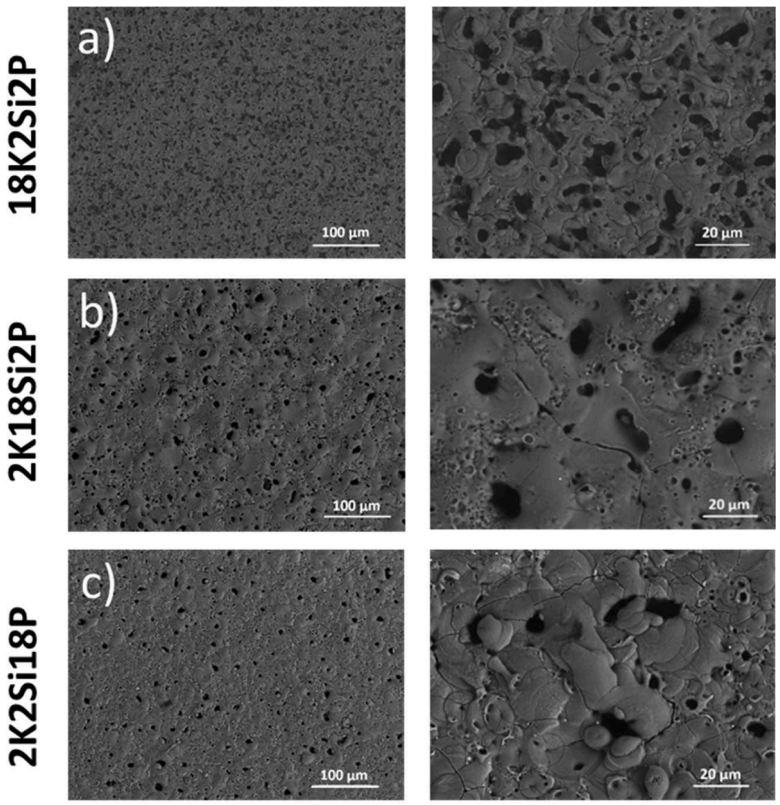

Fig. 6. Surface SEM images of PEO coatings obtained using base electrolytes: 18K2Si2P (a), 2K18Si2P (b), 2K2Si18P (c).

a rough surface of 2.6 ± 0.2 μm with a total porosity of 7.1 ± 1.0% (number of pores equal to 1490 ± 244). Surface characterized by crater- and volcano-like morphological features surrounded by molten electrolyte species. In the P-based electrolyte (2K2Si18P) (Fig. 6(c)), the coating surface has a lowest porosity of 4.4 ± 0.3% (number of pores equal to 1325 ± 256). Mainly crater-like structure with lower pore size of 6.1 ± 0.8 μm in diameter was found.

3.2.2. *Surface morphology for PEO coatings obtained in P-based electrolyte system*

A gradual increase in hydroxide content from 2 to 6 g/L, a crater-like surface structure with large size and nano-sized pores is still observed for the 6K2Si18P coating (Fig. 7(**b**)). This coating has a relative smooth surface (1.3 ± 0.1 μm) with less surface porosity (3.5 ± 0.3%) compared with base 2K2Si18P specimen. However, with an increase in the hydroxide content till 18 g/L (18K2Si18P) (Fig. 7(**c**)), there is a drastic change in the surface morphology, more similar to the 18K2Si2P coating. Surface porosity (15.7 ± 1.1%) as well as number of pores (1770 ± 323) increased much with an increase in hydroxide content. Mainly, a volcano-like structure with large sizes of open pores (16.3 ± 2.0 μm) is observed for 18K2Si18P.

In the case of an increase in the silicate content, a slight increase in surface roughness till 1.6 ± 0.1 μm, porosity (till 4.7 ± 0.7 μm) and number of pores (1592 ± 287) was registered for 2K6Si18P coating (Fig. 7(**d**)) compared to the base 2K2Si18P. With further increase of the Si content (2K18Si18P specimen), the surface morphology changes completely (Fig. 7(e)). The coating is not uniform, and a higher roughness of 4.6 ± 1.2 μm with island-like surface morphology is determined. An approximate surface porosity of 12.9 ± 2.3% was calculated.

3.2.3. *Surface morphology for PEO coatings obtained in Si-based electrolyte system*

An increase in the phosphate content in Si-based electrolyte system resulted in the decrease of surface porosity from 7.1 ± 1.0% to 5.4 ± 0.6% (number of pores 1095 ± 175) for the 2K18Si6P coating (Fig. 8 (**b**)). However, the size of pores increases till 9.3 ± 0.4 μm for 2K18Si6P as well as surface roughness (3.6 ± 0.5 μm) compared to base 2K18Si2P system. With a large increase in the Si content in the electrolyte, the situation is similar to the 2K18Si18P described above (Fig. 8(c)).

3.2.4. *Surface morphology for PEO coatings obtained in mixed electrolyte system*

In the group with an equally increasing concentrations of Si and P, two specimens (2K12Si12P, 2K24Si24P) have showed typical PEO coating morphology in contrast to 2K18Si18P. In 2K12Si12P (Fig. 9(**a**)), the coating surface is relatively flat, with a surface roughness of 2.5 ± 0.7 μm. The coating contains a large size of pores of 7.9 ± 0.9 μm (number of pores equal 1115 ± 209) with crater-like structure. Differently, for the 2K24Si24P specimen (Fig. 9(**c**)), the surface porosity value almost didn't change (5.4 ± 0.9%), but the number of pores even decreased to 569 ± 148. However, the size of pores (17.6 ± 2.5 μm) as well as the surface roughness (5.2 ± 0.2 μm) is increased twice in 2K24Si24P compared to 2K12Si12P. The damages from the arcing PEO processing were also observed at the corners of the 2K24Si24P specimen, which may indicate the formation of a secondary PEO layer, due to appearance of white localized large discharges. With the rapid coating growth associated with the relatively high pH and conductivity, the relatively low voltage leads to intermittent sparking, and the formation of the coating can be very variable. In the case of 2K18Si18P system (Fig. 9(**b**)), it might be related to the transition from crystalline to an amorphous structure supported by the high Si and P content and lower melting temperature of coating phase. The surface tension of the melt on the surface under these conditions prevents uniform distribution of molten volume over the surface, resulting in preferred island-like morphology. However, the increase of the concentration of Si and P can improve the coating formation and surface morphology, but causes other problems associated with arc discharges (2K24Si24P).

At the lowest concentration of species in PEO bath (2K2Si2P) (Fig. 9

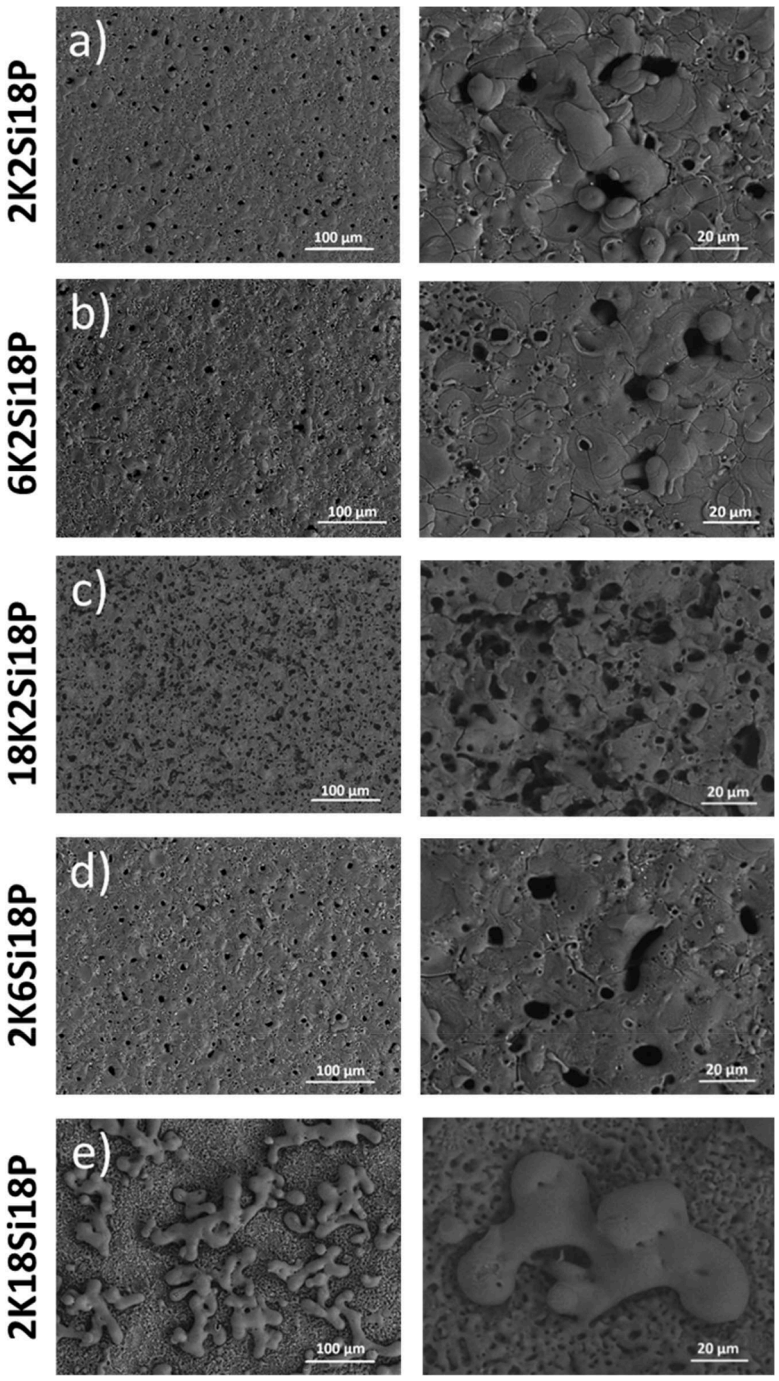

Fig. 7. Surface SEM images of PEO coatings obtained using P-based electrolyte system: with increasing concentration of hydroxide - 2K2Si18P (a), 6K2Si18P (b), 18K2Si18P (c), and with increasing concentration of silicate - 2K6Si18P (d), 2K18Si18P (e).

(**d**)), a high porosity (11.0 ± 1.8%) and elongated pores of 16.2 ± 1.8 μm are observed. For the 6K6Si6P coating (Fig. 9(**e**)), the surface morphology changes completely. Mainly, crater-like structures with open pores were the main feature of these coatings. A smooth and compact coating with the lowest value of surface roughness (1.3 ± 0.2 μm), porosity (2.8 ± 0.2%) and size of pores (4.7 ± 0.5 μm) is noticed. However, the number of pores on the surface of these coatings remains approximately constant (1130 ± 188). The coating 18K18Si18P reveals a crater-like structure with large sized pores (17.9 ± 1.9) (Fig. 9(**f**)). Moreover, a surface is relatively rough (5.3 ± 0.4 μm) and overall porous (6.8 ± 0.7%).

3.2.5. Surface elemental (EDS) analysis of different PEO coatings

Table 2 provides the surface composition of PEO coatings from EDS analysis. It can be seen, the main components of coatings are O, Al, Si, and only a small amount of P is incorporated into the surface. The amount of O was relatively constant for the different coatings.

In Si-based electrolyte as well as in the systems with high Si content (from 6 g/L to 24 g/L), an increase of the Si amount in the coating composition is observed. An increase in the Si content led to a reduced Al incorporation in the coating, due to the formation of phases enriched with Si. The highest Si value of 25.3 ± 0.9 at.% was reached for 2K24Si24P coating. In P-based electrolyte systems even with the highest phosphate content in the treatment bath, the surface composition still has a higher level of Si than P. Surprisingly, the highest level of *P* of

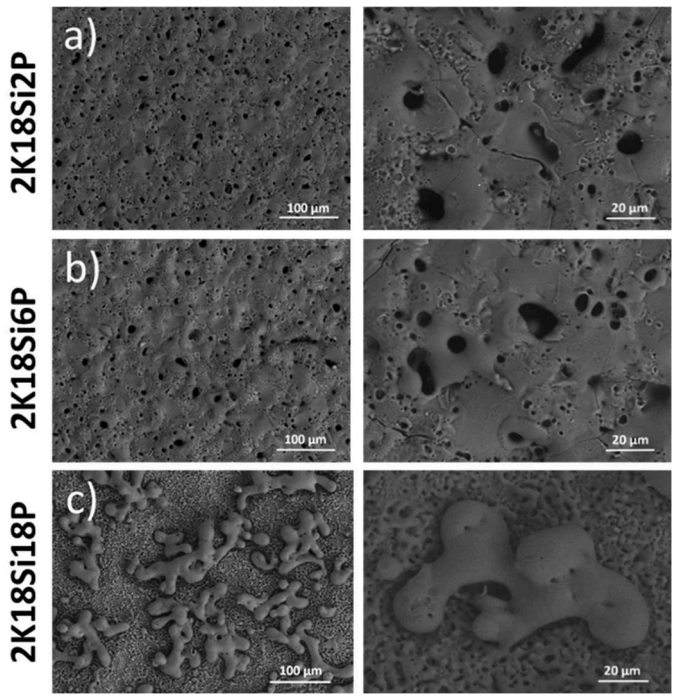

Fig. 8. Surface SEM images of PEO coatings obtained using Si-based electrolyte system with increasing concentration of phosphate - 2K18Si2P (a), 2K18Si6P (b), 2K18Si18P (c).

around 1.9 ± 0.3 at.% is found in the 2K2Si2P coating. Moreover, in P-based electrolyte system, an increase of the hydroxide content (6 till 18 g/L), reduces the content of both P and Si in the coating. The difference in the Si and P amount in the layer might also be a result of differences in reactivity of SiO_3^{2-} and PO_4^{3-} species with substrate ions [44]. Only a relatively small amount of copper is present on the surface, since most of it remains in the substrate, having little effect on the surface treatment. Respective elemental analysis for different PEO coatings shown in **Fig. SI-1**.

The last column in the Table shows the expected phase formation, calculated from the ratio of the elements in the PEO layer. The results show that as soon as Si content in the mixed electrolyte reaches 6 g/L, some silicate phases (mullite/amorphous) starts to form, since an overestimated silicon content is observed. In addition, in the specimens with an amorphous phase (2K18Si18P, 2K24Si24P and 18K18Si18P), some silicate phases might be present, probably also in the form of mullite.

3.3. Cross-sectional morphology and elemental distribution

3.3.1. Cross-sectional morphology and elemental distribution for PEO coatings obtained in base electrolytes

Cross-sectional morphology of the PEO coatings obtained in base electrolytes shown in Fig. 10 (additionally given in **Fig. SI-2**). The growth rate is the highest in the 2K18Si2P coating (ca. 1.1 ± 0.2 µm/min) (Fig. 10(**b**)). Cross-sectional observation for this specimen shows that in spite the outer layer is denser, the pore band tends to be formed inside the coating. For the 18K2Si2P and 2K2Si18P coatings growth rate of about 0.9 ± 0.2 µm/min and 0.6 ± 0.1 µm/min was determined, respectively. Cross-sectional analysis of 18K2Si2P specimen shows that the coating has numerous structural defects, and it is not uniform (Fig. 10(**a**)). In 2K2Si18P, more uniform coating was observed compared to others, although there are still some cavities in the intermediate layer (Fig. 10(**c**)).

The distribution of the main PEO coating forming elements (Al, Si, P) reveals that in 18K2Si2P, Si is mainly located in top layer of the coating in limited amount (Fig. 10(**a**)), whereas almost no P intensity is visible throughout the layer. For 2K18Si2P, Si is distributed relatively uniformly in the layer with some trends to locate at regions closer to the coating surface and around the pores and holes within the coating. P signal intensity for this coating is not detectable (Fig. 10(b)). Contrary, for 2K2Si18P coating, intensive P signal localized at the coating/substrate interface can be detected, while less intensive Si signal is visible around the pores (Fig. 10(**c**)).

3.3.2. Cross-sectional morphology and elemental distribution for PEO coatings obtained in P-based electrolyte system

Obviously, there is an increase of the coating thickness with an increase of electrolyte concentrations in the electrolyte. With an increase of hydroxide content in P-based electrolyte, the coating growth rate increased slowly, from 0.6 ± 0.1 µm/min for the standard electrolyte 2K2SI18P to 0.8 ± 0.1 µm/min for 6K2Si18P (Fig. 11(**b**)) till only 0.9 ±

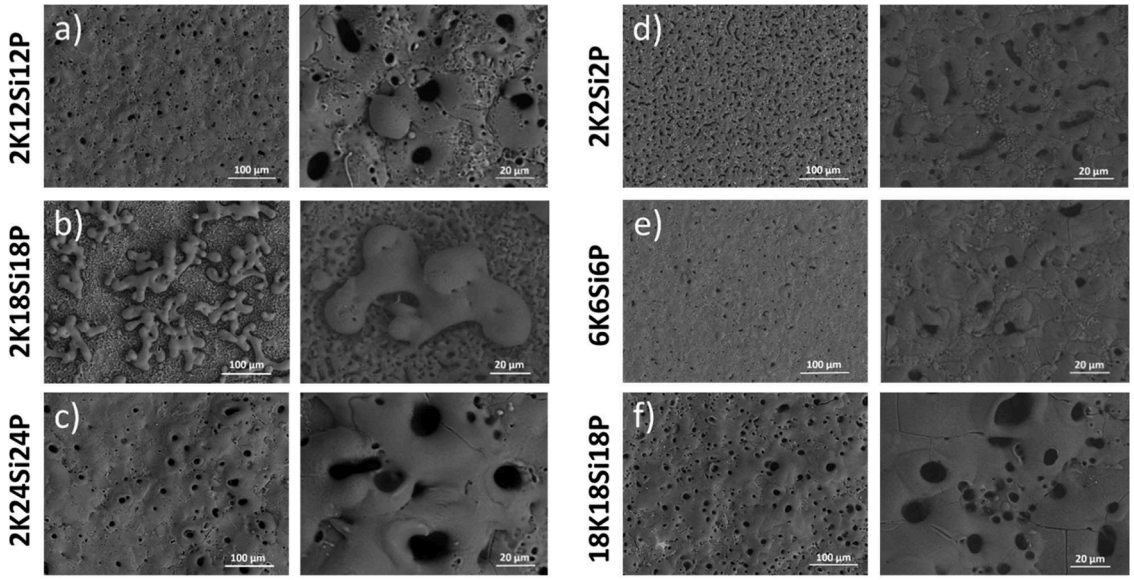

Fig. 9. Surface SEM images of PEO coatings obtained using mixed electrolyte system: with increasing concentration of phosphate and silicate - 2K12Si12P (a), 2K18Si18P (b), 2K24Si24P (c), with increasing concentration of OH:Si:P - 2K2Si2P (d), 6K6Si6P (e), 18K18Si18P (f).

Table 2
Elemental composition (in at.%) of the PEO coatings obtained via EDS analysis.

Sample/elements	Al	O	Si	P	Na	K	Cu	expected formed phases
2K2Si18P	43.9 ± 1.2	52.9 ± 0.7	1.6 ± 0.1	0.5 ± 0.1	0.7 ± 0.1	0.1 ± 0.3	0.2 ± 0.1	Al_2O_3
2K6Si18P	31.9 ± 0.9	54.1 ± 0.4	10.6 ± 0.7	1.5 ± 0.2	1.2 ± 0.1	0.4 ± 0.2	0.3 ± 0.1	Al_2O_3 + mullite
2K12Si12P	24.4 ± 0.6	52.7 ± 0.6	19.4 ± 0.6	1.9 ± 0.2	1.1 ± 0.1	0.3 ± 0.1	0.2 ± 0.2	mullite
2K18Si18P	30.5 ± 0.8	54.3 ± 0.7	11.6 ± 0.4	1.4 ± 0.5	0.9 ± 0.1	0.1 ± 0.1	1.1 ± 0.2	Silicate phase
2K24Si24P	17.7 ± 0.2	51.4 ± 1.1	25.3 ± 0.9	1.8 ± 0.3	3.1 ± 0.3	0.5 ± 0.1	0.3 ± 0.1	Silicate phase
2K2Si2P	41.6 ± 0.9	50.2 ± 0.7	3.4 ± 0.1	1.9 ± 0.3	0.4 ± 0.1	0.7 ± 0.1	1.8 ± 0.2	Al_2O_3
6K6Si6P	35.2 ± 0.5	49.0 ± 0.8	11.2 ± 0.6	0.9 ± 0.2	1.1 ± 0.2	1.0 ± 0.2	1.6 ± 0.2	Al_2O_3 + mullite
18K18Si18P	27.0 ± 0.3	50.8 ± 1.0	14.8 ± 0.7	1.3 ± 0.3	1.9 ± 0.1	2.3 ± 0.2	1.8 ± 0.3	Silicate phase
18K2Si18P	42.9 ± 0.8	52.9 ± 0.9	1.5 ± 0.1	0.7 ± 0.1	0.9 ± 0.1	0.6 ± 0.1	0.6 ± 0.2	Al_2O_3
18K2Si2P	46.9 ± 0.7	48.4 ± 0.3	1.5 ± 0.1	0.2 ± 0.3	0.3 ± 0.1	0.6 ± 0.1	2.1 ± 0.1	Al_2O_3
6K2Si18P	43.2 ± 0.6	52.4 ± 0.5	2.0 ± 0.1	0.6 ± 0.3	0.7 ± 0.1	0.4 ± 0.1	0.2 ± 0.2	Al_2O_3
2K18Si6P	20.6 ± 0.4	51.7 ± 0.9	24.2 ± 0.6	1.1 ± 0.6	1.8 ± 0.1	0.5 ± 0.1	0.2 ± 0.2	mullite
2K18Si2P	22.1 ± 0.6	50.3 ± 0.6	23.8 ± 0.9	0.5 ± 0.4	1.8 ± 0.2	0.7 ± 0.1	0.8 ± 0.2	mullite

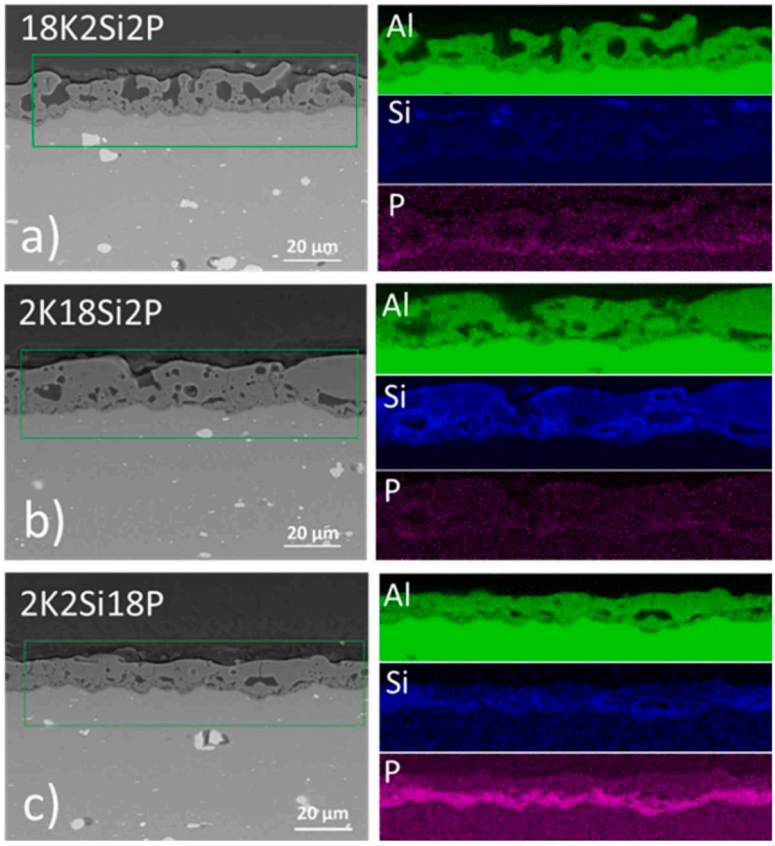

Fig. 10. EDS elemental mapping from cross-sections of PEO coatings formed in base electrolytes: 18K2Si2P (a), 2K18Si2P (b), and 2K2Si18P (c).

0.2 µm/min for 18K2Si18P coatings (Fig. 11(**c**)). However, there is an increase in the size and number of connected pores and holes within the coating with an increase of hydroxide concentration.

With an increase of the silicate concentration in the electrolyte bath, the 2K6Si18P coating has a growth rate of 0.8 ± 0.2 µm/min (Fig. 11**1** (**d**)). Cross-sectional morphology demonstrates more uniform coating with connected pores in coating/substrate region, similar to base 2K2Si18P layer. However, a further increase of silicate concentration till 18 g/L does not allow a uniform coating growth (Fig. 11(**e**)). The formed islands reach thickness of 30 ± 4 µm, while the surrounding areas are only around 1 µm thick.

Overall, EDS elemental mappings, obtained on the cross-sections of PEO coatings, show that with an increase of the hydroxide content in the treatment bath, the intensity of both Si and P signals at the coating/substrate interface decreases and more homogeneous elemental distribution over the coating can be observed (Fig. 11(c)). An increase of silicate in the treatment bath leads to an increase of the Si intensity throughout the coating, mainly around pores and at the top layer of the coating (Fig. 11(d)).

3.3.3. Cross-sectional morphology and elemental distribution for PEO coatings obtained in Si-based electrolyte system

The coatings grow faster in Si-based electrolyte systems (Fig. 12(a), (b)) compared to those obtained in phosphate ones. A little increase of the phosphate content (2K18Si6P specimen) results in the rise of the coating growth rate till 1.2 ± 0.2 µm/min after 20 min of processing. However, there are many small sized pores and holes in the resulting layer and overall coating is not dense.

Overall, for this group of specimens, the elemental distribution maps obtained on the coating cross-sections, reveal that an increase of phosphate in the coating composition leads to an increase of the P signal intensity (Fig. 12(a)–(c)). Also noticed is a high Si intensity especially at

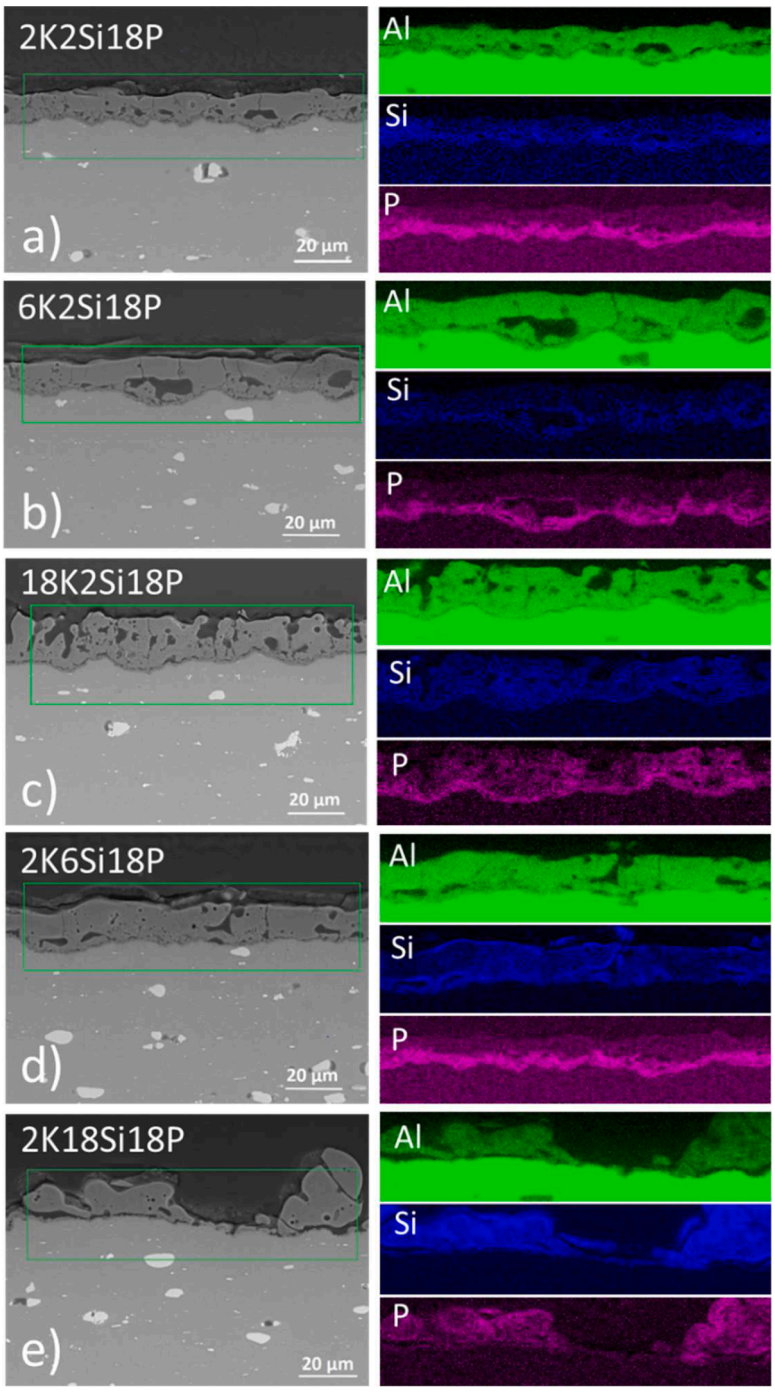

Fig. 11. EDS elemental mapping from cross-sections of PEO coatings formed in P-based electrolyte system: with increasing concentration of hydroxide - 2K2Si18P (a), 6K2Si18P (b), 18K2Si18P (c), and with increasing concentration of silicate - 2K6Si18P (d), 2K18Si18P (e).

the top layer of the coating which increases with an increase in phosphate content (Fig. 12(b)).

3.3.4. Cross-sectional morphology and elemental distribution for PEO coatings obtained in mixed electrolyte system

With an increase of Si and P concentration simultaneously, the coatings grow homogeneously, and thickness increase is significant (Fig. 13(a) and (**c**)). The coating growth rate sharply increase from 1.3 ± 0.2 μm/min for 2K12Si12P system till 2.1 ± 0.3 μm/min for 2K24Si24P system. Overall, dense and uniform coatings with fewer pores are observed in this group of treatments. However, there are problems with stationary discharges for the 2K24Si24P and the coating formation problems seen for the 2K18Si18P are not fully solved (Fig. 13 (b)).

The lowest growth rate was demonstrated for the 2K2Si2P coating (ca. 0.5 ± 0.2 μm/min) (Fig. 13(d)). The numerous connected different sized pores at the coating/substrate interface are also presented. The high growth rate (ca. 2.0 ± 0.4 μm/min) results in a thick and dense coating obtained in the 18K18Si18P electrolyte (Fig. 13(f)).

Fig. 14 summaries the coating thickness as a function of electrolyte concentrations for different PEO layers. One can see that Si-based electrolyte systems boost the coating growth as well as higher content of silicate in the mixed electrolytes with phosphate, except for 2K18Si18P system.

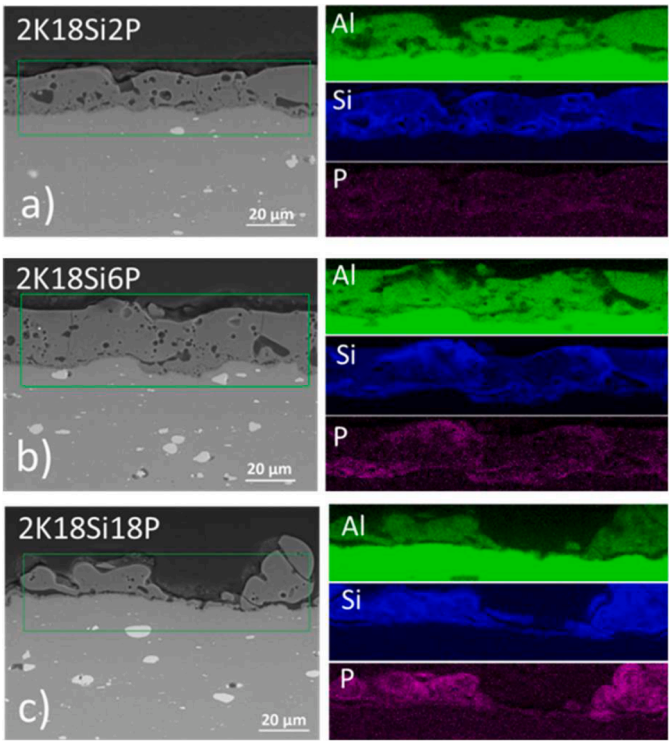

Fig. 12. EDS elemental mapping from cross-sections of PEO coatings formed in Si-based electrolyte system with increasing concentration of P 2K18Si2P (a), 2K18Si6P (b), 2K18Si18P (c).

Fig. 15 shows a cross-section view of the coatings obtained in base electrolytes (18K2Si2P, 2K18Si2P, 2K2Si18P) and one thicker coating with fully amorphous phase (18K18Si18P). The growth direction of PEO layer (inwards/outwards) is analysed. Results demonstrate that the coatings obtained in OH-, and P-based electrolytes mainly grows towards the substrate (Fig. 15(a), (**c**)), while the predominant outward growth of the coating is observed in the coating obtained in the Si-based electrolyte (Fig. 15(**b**)). For 18K18Si18P coating, high outward growth is also dominant (Fig. 15(d)). Additionally, **Table SI-2** (in SI) shows the results of measuring the whole thickness (by SEM cross section) and the outer layer thickness of the coatings (by laser scanning and optical microscopes) for all specimens (except 2K18Si18P). The measurements were carried out by focusing and determining the difference in heights of the bare substrate and the coated area. However, the specimens not being perfectly straight or flat, and they could not be perfectly vertical, so they were slightly tilted during measurement. Which may explain the differences in results between the LSM and optical microscopes, and the inherent roughness in PEO coating surface does not allow to obtain exact figures as well. Comparing the results from **Table SI-2** and Fig. 15, it is assumed that the results obtained with LSM are closer to those presented in the figures above. Since, the coatings obtained in Si-based electrolyte and with a high content of silicates show the mainly outward growth. However, for coatings obtained in OH- and P-based electrolytes, the results from the table don't exactly match the figures above (Fig. 15(a), (c)), which show of about 50/50 growth in both directions for the 18K2Si2P specimen, and more outward growth in 2K2Si18P.

3.3.5. Elemental distribution through PEO coating obtained in different electrolytes

Table SI-3 shows the EDS elemental composition of the coatings (Al, O, Si and P) taken from the cross sections at three different locations, namely close to the surface, centre and close to the interface to the substrate. At the lowest electrolyte concentration (2K2Si2P), PEO coatings have a relative low but uniform distribution of the Si species. With increase of electrolyte concentration, for the PEO coatings obtained in various ternary electrolyte systems at lower electrolyte concentrations (from 6 till 12 g/L of respective components), Si and P elements are mostly enriched at the coating/substrate interface. Contrary, for the PEO layers obtained from the higher concentrated electrolytes (especially in Si/P mixtures with concentrations between 18 and 24 g/L of respective components), this trend changes and Si-containing species are mostly located closer to the surface. P is much more enriched at the coating/substrate interface as one would expect from the low concentration in the electrolyte compared to high concentrations in the electrolyte.

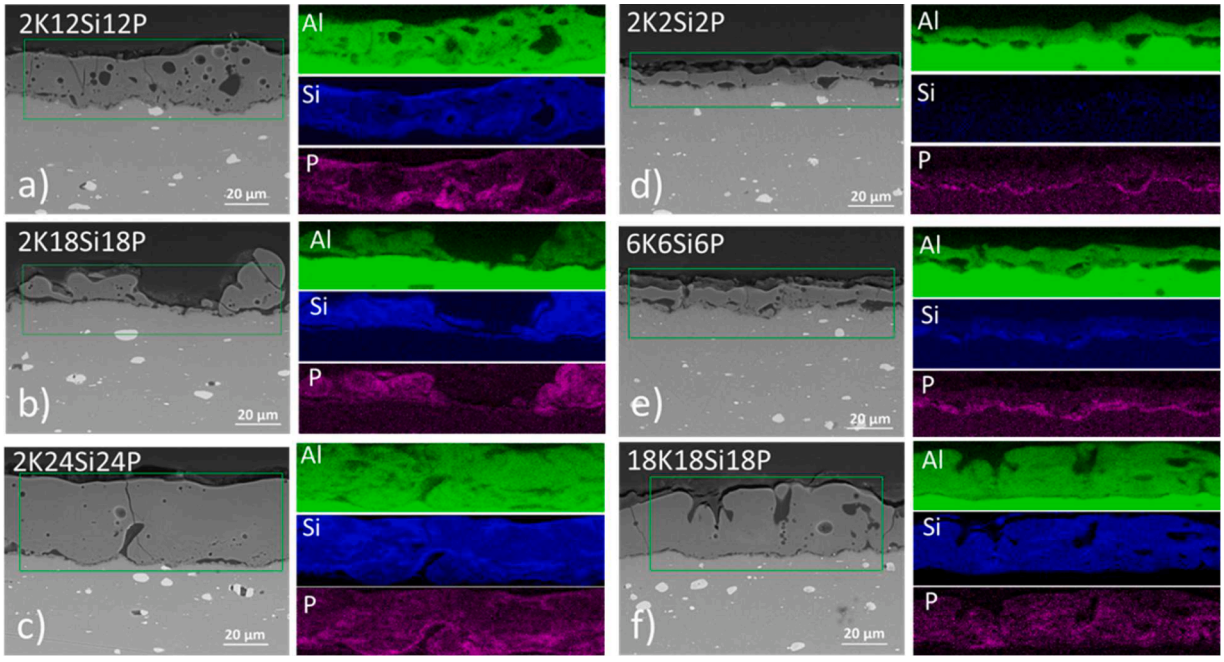

Fig. 13. EDS elemental mapping from cross-sections of PEO coatings formed in mixed electrolyte system: with increasing concentration of phosphate and silicate - 2K12Si12P (a), 2K18Si18P (b), 2K24Si24P (c), with increasing concentration of OH:Si:P - 2K2Si2P (d), 6K6Si6P (e), 18K18Si18P (f).

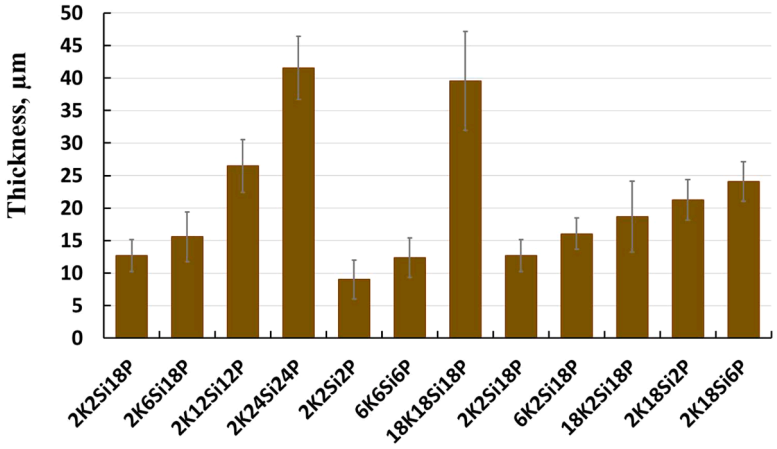

Fig. 14. Average thicknesses as a function of the electrolyte concentrations for different PEO coatings.

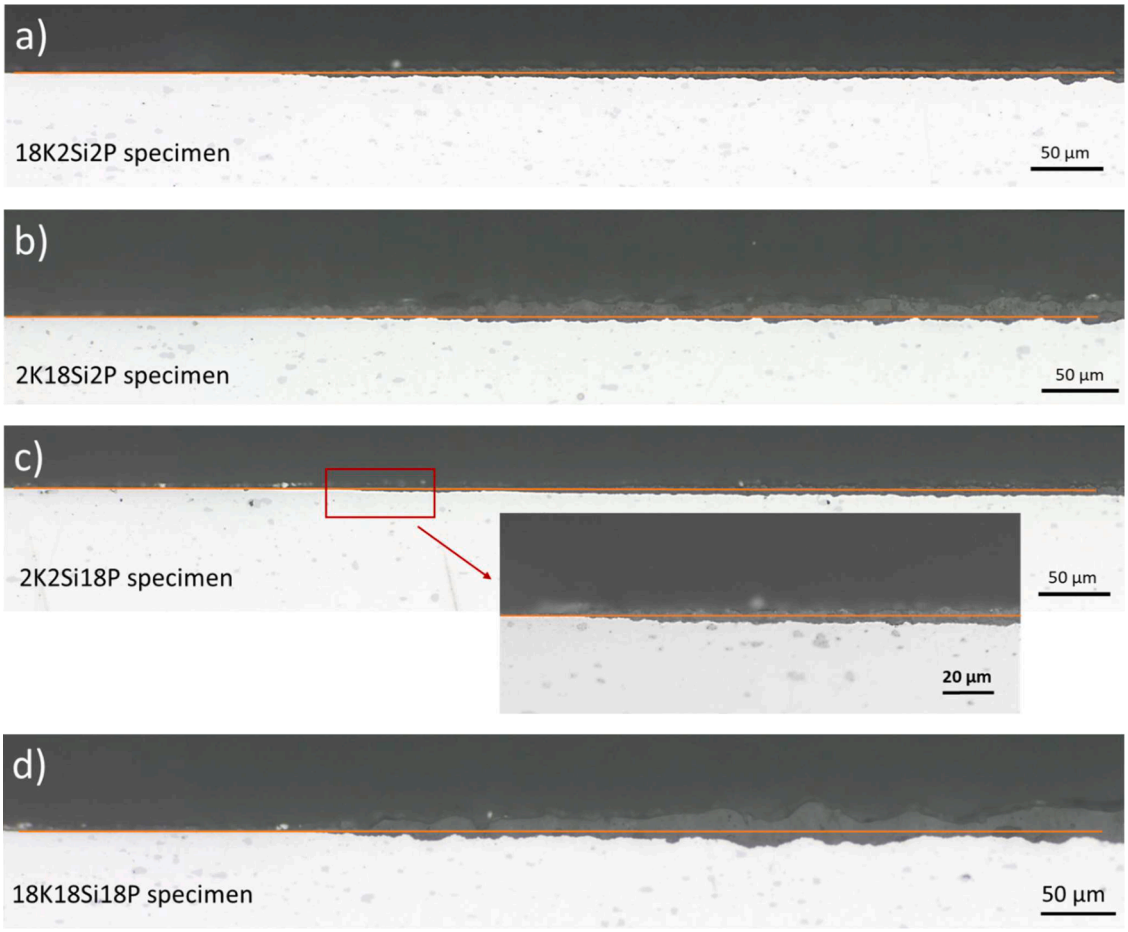

Fig. 15. Optical cross-section views of 18K2Si2P (a), 2K18Si2P (b), 2K2Si18P (c) and 18K18Si18P (d) coatings.

Glow discharge optical emission spectroscopy (GDOES) was used in order to get more integral information of the elements distribution across the PEO coatings (Figs. 16–18, **SI-3**). During the respective measurements, signal intensities have direct relations to the amount of the element and sputtering time can be correlated with depth of the sputtering (coating thickness). Main elements presented in the PEO coatings are Al, O, Si and P. The copper signal appears only after beginning of bulk alloy sputtering and used for additional control of the coating/substrate interface.

All the PEO-coated samples demonstrate three main regions during the sputtering. The first zone is PEO-coating. This region sputters first and commonly consists of aluminium, oxygen and electrolyte-containing elements (P, Si). The second region is related to coating/substrate interface. The duration of this period (and respective thickness of this layer) depends mainly on the roughness of the interface and on inhomogeneity of the PEO-coating. During the sputtering, the oxygen signal intensity from PEO layer is decreasing, while the aluminium and copper signals from substrate are increasing. Additional feature of the region is a high amount of phosphorus. One can see from Figs. 16 to 18, **SI-3** that before decreasing to background level, intensity of P-signal

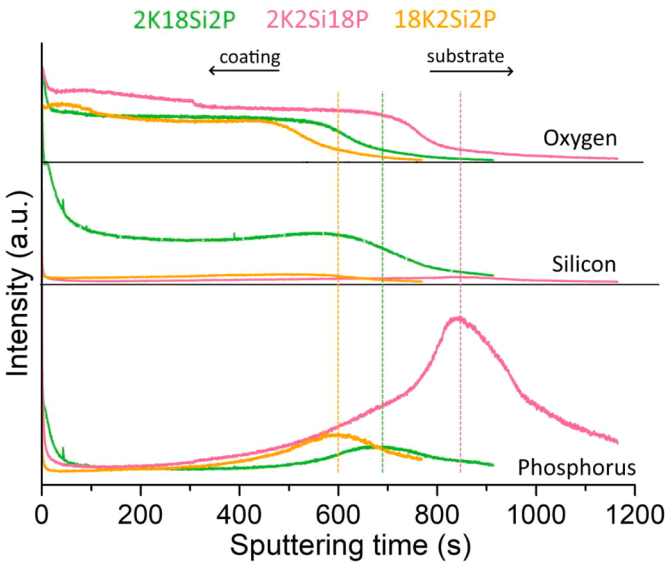

Fig. 16. GDOES-depth profile of PEO-coated specimens formed in base electrolytes.

grows and forms a kind of peak. It matches well with the results, demonstrated by EDS mapping (Figs. 10–13) and EDS area analysis (**Table SI-3** (in SI)). Formation of the P-rich layer can be explained via the diffusion of the electrolyte species to the substrate through initially formed oxide layer.

In P-based electrolyte systems, an increase of the hydroxide and Si concentration contributes to a decrease of the intensity of P signal at the interface, but an increase in the surface is observed (Fig. 17). This result correlates well with observations in **Table SI-3**.

The results also confirm an increase in the sputtering time with an increase in the concentration of electrolytes in the systems, which corresponds to an increase in the coating thickness. As shown earlier, the thickest coatings correspond to the Si-based electrolyte and the mixed electrolyte systems with high silicate concentration with the longest sputtering time, respectively, except of 2K18Si18P. The untypical coating formation for 2K18Si18P specimen is shown during GDOES sputtering (Fig. 17(b)). The observed coating zone looks shorter, which might be associated with uneven coating structure. A higher P signal in the coating surface region and lower intensity at the interface is found for 2K18Si18P specimen. Si signal intensity also increases closer the surface area during the coating sputtering.

Relatively uniform distribution of Si and P intensities over the coating depth is registered during the sputtering of specimens produced in the group of mixed electrolytes with high concentration of silicate and

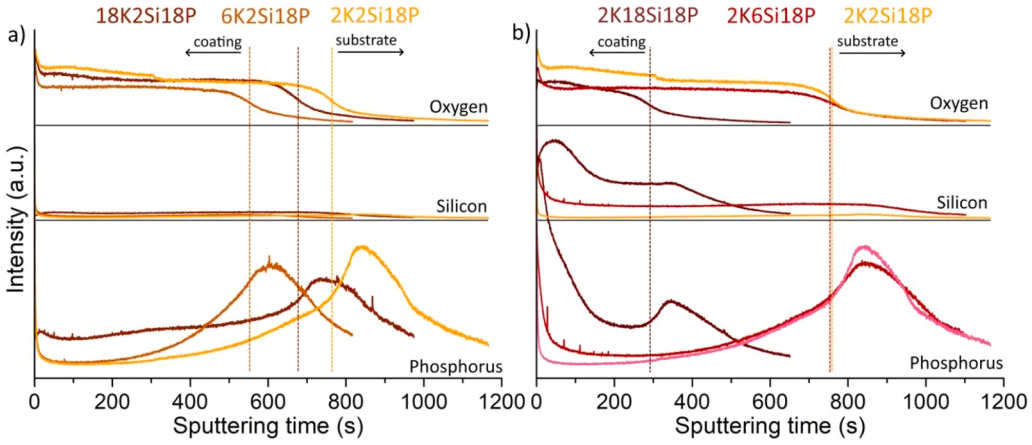

Fig. 17. GDOES-depth profile of PEO-coated specimens formed in P-based electrolyte system.

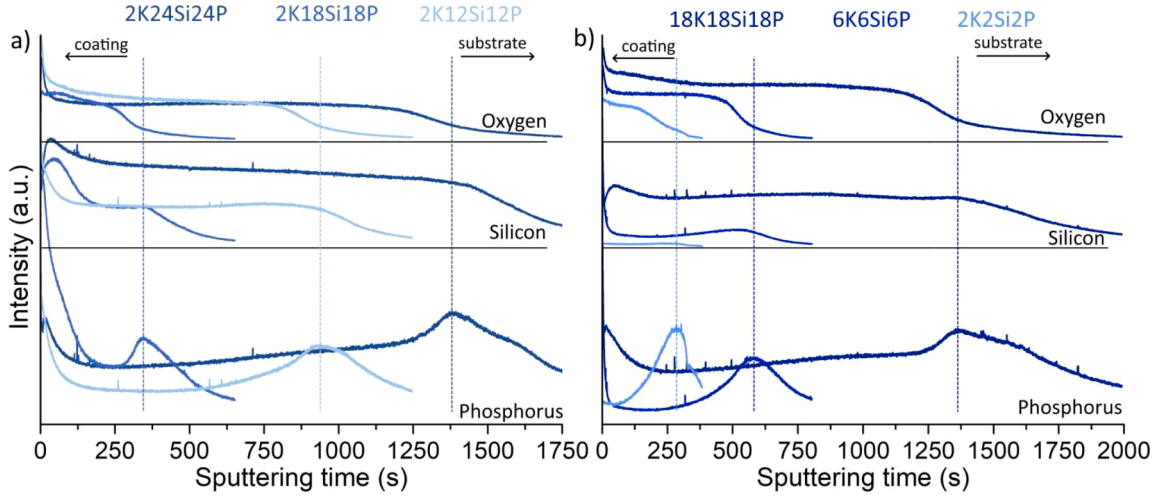

Fig. 18. GDOES-depth profile of PEO-coated specimens formed in mixed electrolyte system: with equally increasing silicate and phosphate concentrations (a), and equally increasing hydroxide, silicate and phosphate concentrations (b).

phosphate (18–24 g/L) (Fig. 18). This observation matches nicely with EDS mapping analysis Fig. 13(b), (c), (f).

For all patterns, obtained during GDOES sputtering, the last region of the sputtering is associated to the bulk alloy. This region has signals only of copper and aluminium elements from the AA2024 alloy. The rest of elements demonstrate only signals close to background level.

3.4. Phase composition and distribution

3.4.1. Phase composition for PEO coatings obtained in base electrolytes

XRD patterns of PEO coatings on AA2024 produced in base electrolytes presents in Fig. 19. For all the coatings, only a small amount of α-Al_2O_3 can be found. It can be explained in a way, that the applied current density and resulting discharge voltage was not enough to cause phase transformation from γ-Al_2O_3 to α-Al_2O_3 (starts at around 1000 °C [17]). One can see that for the coatings obtained in OH-based electrolyte (18K2Si2P) the PEO layer consists of crystalline compounds, mainly γ-Al_2O_3 (ICDD card 00-010-0425) and small amount of α-Al_2O_3 (ICDD card 00-046-1212). The treatment in Si-based electrolyte (2K18Si2P) resulted in a mixed coating phase composition, containing both crystalline and amorphous structures. A broad halo at 2θ between 15° and 35° in the XRD pattern can represent an amorphous phase. The main crystalline phase was determined as mullite ($3Al_2O_3{\cdot}2SiO_2$) (ICDD card 01-079-1454) and small amount of γ-Al_2O_3 and α-Al_2O_3 were visible. This result demonstrates a significant contribution of silicate-based compounds from electrolyte in the coating formation process. The coatings obtained in P-reached electrolyte (2K2Si18P) consists of similar crystalline phases as the one obtained in OH-based electrolyte (γ-Al_2O_3 and α-Al_2O_3), indicating that substrate oxidation plays a dominant role in the formation mechanism.

3.4.2. Phase composition for PEO coatings obtained in P-based electrolyte system

Analysing the XRD patterns of coatings obtained in P-based electrolytes with a gradual increase of the hydroxide content (Fig. 20(a)), there is a broadening of the γ-Al_2O_3 associated diffraction, while the α-Al_2O_3 peaks almost disappear for higher concentrated electrolytes (18K2Si18P). It can be due to a reduced crystalline size in the coating structure. A gradual increase of the silicate content (2K6Si18P) results, in a similar γ-Al_2O_3 peak broadening, while almost no peaks associated to α-Al_2O_3 can be observed (Fig. 20(b)). An amorphous phase starts to form noticeably when the silicate concentration in the electrolyte is equal or higher than 6 g/L despite of the phosphate concentration. At the highest concentrations of silicates (18 g/L), a fully amorphous coating is reached (2K18Si18P).

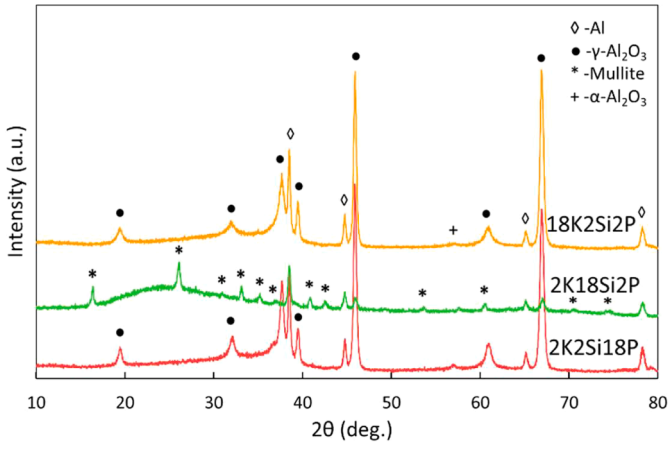

Fig. 19. X-ray diffraction patterns of different PEO coatings formed in base electrolytes.

3.4.3. Phase composition for PEO coatings obtained in Si-based electrolyte system

In Si-based electrolyte systems, with a gradual increase of the phosphate content, at the lower concentration of phosphates (2K18Si2P, 2K18Si6P), the coatings consist of both crystalline (mullite, γ-Al_2O_3, α-Al_2O_3) and amorphous compound (Fig. 21). With an increase of phosphate concentration, broadening or reduction of mullite and γ-Al_2O_3 peaks are observed. A further increase of the phosphate content (2K18Si18P) in the treatment bath contributes to a fully amorphous phase in the coating composition.

3.4.4. Phase composition for PEO coatings obtained in mixed electrolyte system

With an equally increasing content of Si and P in mixed electrolytes, the XRD patterns demonstrate, that the coating formed in 2K12Si12P electrolyte consists of amorphous and crystalline phases, where mullite crystalline phase is dominant (Fig. 22(a)). Mainly amorphous coating can be obtained in the electrolytes with higher silicate and phosphate concentrations (18–24 g/L). For those coatings no peaks of mullite are visible.

A gradual equal increase of all three components (Fig. 22(b)), the PEO coating obtained in electrolyte with lowest concentration (2K2Si2P) contains mainly crystalline phases (γ-Al_2O_3 and α-Al_2O_3). For the coating obtained in 6K6Si6P electrolyte, the crystalline phase peaks broaden, and at the highest concentrations of electrolytes (18K18Si18P), the coatings are mainly composed of amorphous phases.

The variations of the coating thickness and phase composition as a function of silicate and phosphate concentrations in the electrolytes with fixed (2 g/L) concentration of hydroxide are visualized in Fig. 23. The concentration of phosphate does not provide a noticeable effect on the phase composition of the coating. The PEO layers, obtained either with 2 g/L or with 18 g/L of phosphates, mostly consists of γ-Al_2O_3. The increase of silicate concentration in electrolyte results in coatings with amorphous and mullite crystal structure, while simultaneous increase of silicates and phosphates above 18 g/L end up with mostly amorphous coatings. This observation can be explained in a way, that the rapid solidification of alumina promotes the formation of metastable γ-Al_2O_3 phase, when the dissolution of Al is accelerated in P-based electrolytes. In the Si-based electrolyte, the charged complexes from electrolyte are attracted toward the surface. They decompose on the surface due to the plasma discharges forming molten Al_2O_3 and SiO_2 materials, which further react and form insoluble amorphous mullite-based compounds ($3Al_2O_3{\cdot}2SiO_2$).

With an increase of phosphate concentration in the PEO bath, the formation of amorphous phase dominates. Obviously, the phosphate addition supports the glass forming ability of silicates during processing. It can be speculated, that the coating composition changes and makes it possible to reduce the critical cooling temperatures for amorphization resulting in the retardance of crystal phase formation and domination of amorphous structures.

Overall, when a high final voltage (above 470 V) is reached for coatings with low concentrations of various ternary electrolyte compositions (2 - 6 g/L), the PEO coating composition is dominated by alumina crystalline phases. With high silicate concentrations in the electrolyte, accompanied by an increase of phosphate concentration, the final voltage corresponds to around 455 V. The coating composition in such a case is dominated by amorphous phases in combination with crystalline mullite and alumina. At low final voltages of about 360 V and high silicate and phosphate concentrations, the composition of the coatings consists fully of amorphous phase.

3.4.5. Synchrotron X-ray diffraction analysis for PEO coatings obtained in base electrolytes

To learn more about the phase distribution of the main components within the coating, measurements were performed using the nano-focused X-ray beam at the P03, PETRAIII (DESY, Hamburg). Fig. 24

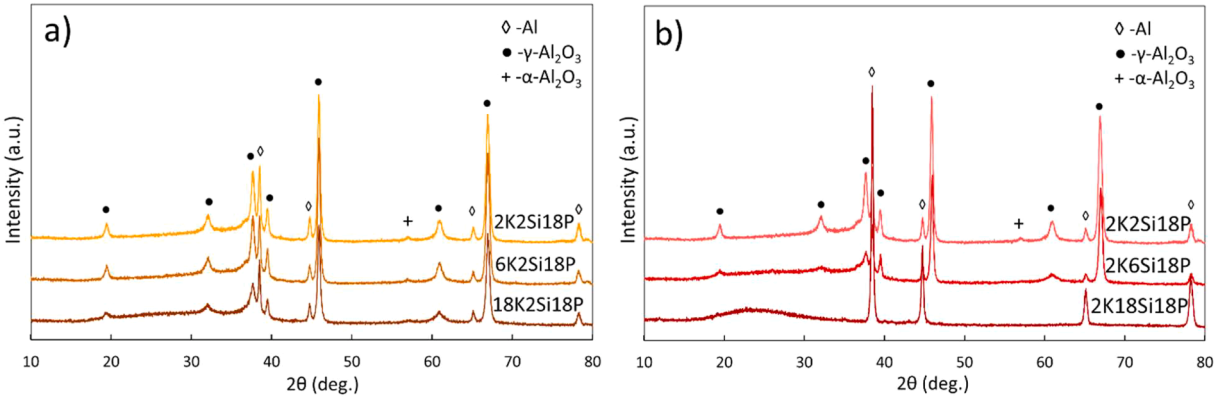

Fig. 20. X-ray diffraction patterns of different PEO coatings formed in P-based electrolyte system with an increase of the hydroxide content (a), with an increase of the silicate content (b).

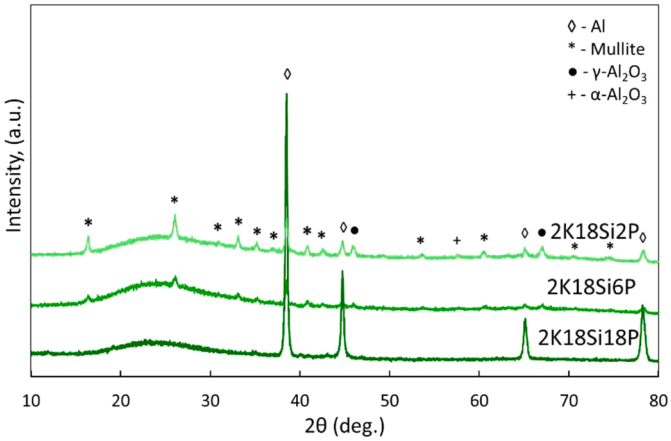

Fig. 21. X-ray diffraction patterns of different PEO coatings formed in Si-based electrolyte system with an increase of the phosphate content.

presents selected localized patterns for the 18K2Si2P, 2K18Si2P, 2K2Si18P specimens. The XRD patterns are taken across the coating from the coating surface to the substrate. Consistent with laboratory (integral) XRD analysis (Figs. 19–22), the results show that γ-Al_2O_3 is a main crystalline phase in both 18K2Si2P and 2K2Si18P coatings (Fig. 24 (a), (c)). However, the intensities of the reflections from those coatings are much higher than from the 2K18Si2P coating, where mullite phase is dominant (Fig. 24(b)). The high-resolution X-ray pattern also shows lower intensity of α-Al_2O_3 as well as some other alumina phases (θ-, β-, δ-, κ-, χ-, Al_2O_3) for 18K2Si2P, 2K18Si2P, 2K2Si18P specimens, which were not detected during laboratory X-ray diffraction analysis. The appearance of several Al_2O_3 phases can be the result of following phase transformations (Eq. (2)):

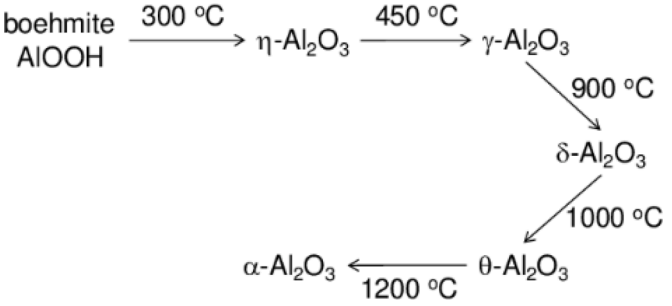

(2)

Two-dimensional phase maps are plotted in **Fig. SI-4** (in SI) to show the spatial phase distribution across the coating thickness with a scan area of 90 × 90 μm. Each image shows the spatial distribution of a specific crystal phase (left column) within a given PEO layer with the respective electrolyte conditions (top row). The colour from blue to yellow indicates the relative amount of the respective crystal phase. The distribution of Al from the substrates is also displayed to illustrate the interface. For both 18K2Si2P and 2K2Si18P coatings, it is evident that γ-Al_2O_3 is the primary phase, which is almost uniformly distributed through the entire thickness of the coating. The overlapping of coating signal with substrate signal may be explained by the surface roughness and not uniform coating thickness, forming a wavy coating/substrate interfaces. However, for 2K18Si2P coating the phase distribution is different, there is only partial distribution of γ-Al_2O_3 phase with lower intensity. This suggests a higher consumption of alumina during the

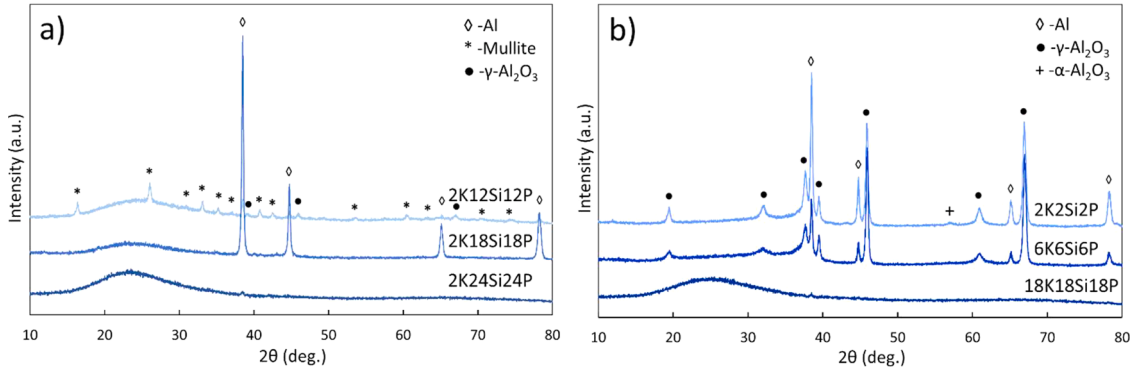

Fig. 22. X-ray diffraction patterns of different PEO coatings formed in mixed electrolyte system: with equally increasing silicate and phosphate concentrations (a), and equally increasing hydroxide, silicate and phosphate concentrations (b).

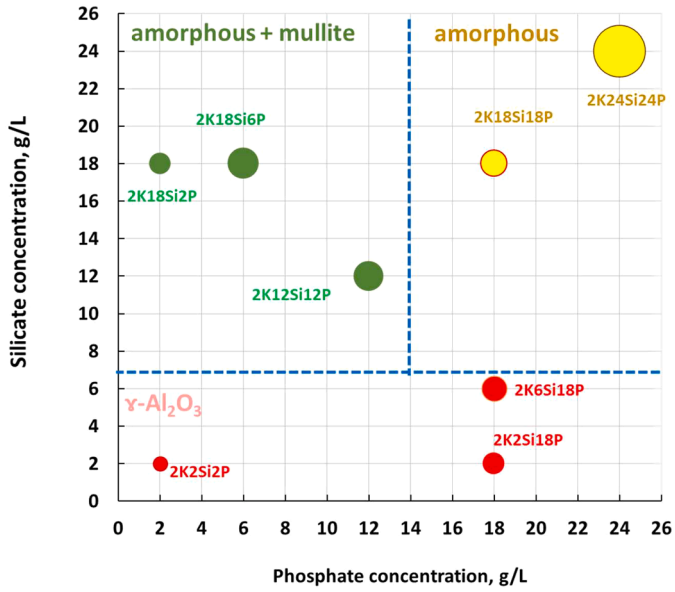

Fig. 23. Influence of silicate and phosphate concentration on coating thickness and phase formation during PEO processing in 2K*x*Si*y*P electrolytes. Diameter of points indicates the coating thickness, while colour represents the different phases. Dash-lines are only guidelines for eyes to indicate the different phase-areas.

reaction with SiO_2 forming mullite phase ($3Al_2O_3{\cdot}2SiO_2$). Mullite, the main 2K18Si2P coating forming phase, has a more intense partial distribution towards the coating surface (**Fig. SI-4(j)**, whereas the γ-Al_2O_3 is located in the intermediate layer (**Fig. SI-4(b)**. The 2K18Si2P coating formation consists of two features compared to 18K2Si2P and 2K2Si18P. Deposition of electrolyte compounds and reaction to mullite occurs at the electrolyte/coating interface; the Al oxidation happens closer to the substrate area. Moreover, α-Al_2O_3 has a relatively lower intensity distribution for all the coatings, that in consistent with lab XRD results (Figs. 19–22). In spite of α-Al_2O_3 is distributed closer to the surface area, there is also its enrichments within the coating thickness, possibly, in regions of strong discharges (**Fig. SI-4(d)**–(**f**)). For 2K2Si18P coating, the distribution of α-Al_2O_3 is quite uniform, indicating lower intensity of localized discharges. This result is in a logical agreement with the visual observation of discharges during PEO processing presented above.

4. Mechanism of PEO formation (discussion)

The effect of electrolyte composition is a superposition of different effects. First, the electrolyte conductivity (resistivity) and its effect on the breakdown voltage. The breakdown voltage of PEO coatings increases linearly with the logarithm of electrolyte resistivity. According to [43], primary electrons, leading to electron avalanches and subsequent breakdown of the oxide layer, are formed in the Helmholtz double layer. The electron injection current at the oxide-electrolyte interface is affected by the electric potential in the Helmholtz double layer [45]. Additionally, the electrochemical potential of electrons in this layer, as well as the field strength at the oxide-electrolyte interface, determine the height of the potential barrier for electron injection from the electrolyte [43].

The second is the mixture related availability of ionic species and its kinetics to form stable phases with/on aluminium and alumina. Various phases are involved in the coating formation process. This compounds have different melting temperature and melt volume, due to the discharges. During oxidation, the main part of the total current through the barrier film is ionic [43]. According to [46], it was suggested that PEO layer formation anions can be divided in 3 group: a) mobile inwards (phosphate, sulphate), b) immobile (borate, silicate) or c) mobile

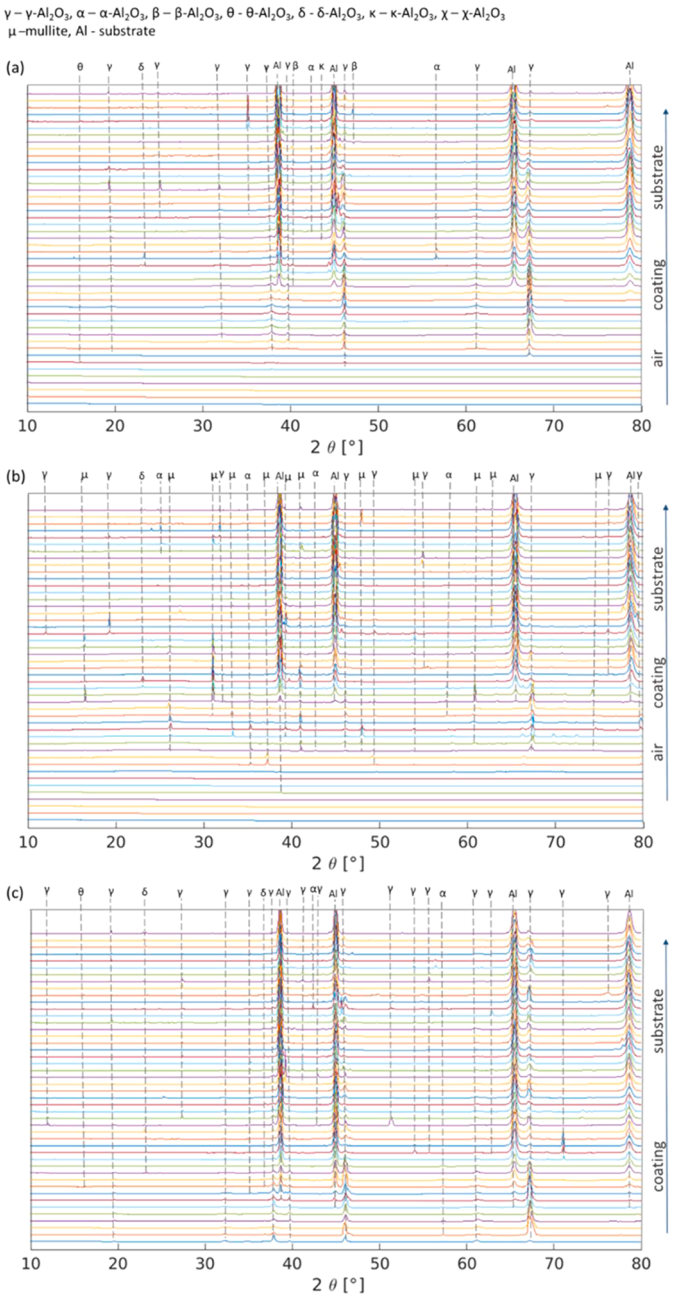

Fig. 24. High-resolution XRD patterns of a selected line perpendicular to the interface in the direction air-coating-substrate for the PEO coatings obtained in: (a) 18K2Si2P, (b) 2K18Si2P and (c) 2K2Si18P electrolytes.

outwards (tungstate, molybdate). The ions from the first group have tendency to incorporate into the layer and migrate inside the coating under electrical field (in the case of phosphates). Presence of aggressive OH- species in the electrolyte provoke dissolution of the alumina and formation of a porous structure. Additionally, incorporation of characteristic anions (such as SiO_3^{2-}, PO_4^{3-}) of the electrolyte are not essential for oxide layer formation, as evidenced by coating growth in OH- and P-based electrolytes. Silicate is initially adsorbed at the coating/electrolyte interface, and incorporated as SiO_2 [47]. Plasma discharges appear with gradual increase of electrical potential. These PEO sparks appear as close as possible to the substrate and due to the high amount of energy, applied during PEO processing, convert the pre-formed oxide layer and form the PEO coating [48].

The third effect is the "survival" of discharge effects until the

maximum reached potentials. The intensity of the process depends on the density and energy of these discharges, which, consequently, can also be determined by the formed coating's characteristics (such as phase composition, mechanical stability) and the thickness of the oxide layer. The thicker the layer is, the less numerous, but more powerful and long-lasting the discharges are. Different types of discharges are strongly associated with different distribution, number and size of pores, holes and cracks in the coating [49,50]. More intense discharges result in the larger pores, while smaller pores can be a result of micro-discharge sparks of less intensity [51,52]. The observed coating morphology can be explained by the model suggested in [50]. It consists of three A-, B- and C-type discharges. In OH-based electrolyte, based on surface morphology observation (Fig. 6(a)), it is assumed that the intense discharges pass through the coating/substrate interface across the discharge channels, where the substrate is oxidized. However, lack of the molten species from the substrate material and electrolyte does not allow to fill all large open pores. Resulting in relatively low thickness and high surface porosity (18K2Si2P, 18K2Si18P).

In Si-based electrolyte, it is likely that all three (A-, B- and C-) type discharges are present. A- and C-type discharges occur at the electrolyte/coating interface with gas inclusion and glow discharge ignition. Enhancement of the PEO coating growth can be explained by silica polycondensation processes, which is facilitated mostly by the more intensive discharge sparks (B-type) [53,54]. Smaller size and number of pores compared to OH-based electrolyte (Fig. 6(a)), but larger than in the coatings from phosphate-based electrolyte (Fig. 6(c)), is observed for PEO layers produced in silicate-based electrolyte (Fig. 6(b)). Since the B-type discharges are the strongest and derive from breakdown voltage in a strong electric field, they would have the highest effect on the microstructure of the coatings. A partial phase distribution with high intensities may also be an evidence for higher local temperatures during the process (**Fig. SI-4(b), (e), (j)**). It is reported that the molten products around the pores correspond to the formed alumina species, while surroundings are enriched with electrolyte constituents [55]. It is expected that former can be formed by stronger B-type discharges, while A-, C-type less intense discharges may be the cause for the latter structural features. In other words, it is likely that the occurrence of B-type discharges can lead to substrate oxidation, while A-, and C-type discharges can cause deposition of species from the electrolyte, and they can consistently dominate the process.

P-based electrolytes were found to be more favourable for obtaining more uniform PEO layers, with smaller size and number of pores compared to others two electrolytes. However, those coatings are not dense inside. Internal residual and thermal stresses and consequently increasing inner pore cavities can be the reason for a minor increase in the thickness of the coatings, despite the high oxidation voltage during the process. A higher discharge voltage in this case may mean a coating consistence of more insulating phases (γ-Al_2O_3). Possibly, most of the energy was released to the electrolyte since no strong destructive discharges were observed, and softer discharges dominated the process. Mainly A- and C-type of discharges are believed to occur. A uniform phase distribution may also indicate a softer PEO process (**Fig. SI-4(c), (f)**).

The electrical energy consumption was calculated by integration of the power as a function of the treatment time (Eq. (3)) [56], for different tested systems (Fig. 25).

$$E = \int_{t_0}^{t} (VI)dt \tag{3}$$

where t_0 and t- start and end times of PEO treatment with a step of 0.01 s, V – voltage value recorded every 0.01 s, I - current density.

A reduction by using highly concentrated electrolytes with a high concentration of silicates and phosphates has been confirmed, which significantly reduces the energy consumption by up to 31% in the case of 18K18Si18P (compared to 2K2Si2P), and a saving of up to 14% in the case of 2K24Si24P (compared to sample 2K12Si12P). The use of Si-based electrolyte (2K18Si2P) saves energy of up to 6% compared to high concentrated phosphate electrolyte (2K2Si18P). In addition, in P-based electrolyte system, increasing the hydroxide content till 18 g/L (18K2Si18P) is beneficial in terms of saving energy consumption up to 25% compared to the base 2K2Si18P. In general, a low concentration of mixed electrolytes as well as a *P*-based electrolyte leads to consume more energy in the mixed electrolyte system.

To summarize, the main characteristics of PEO coatings obtained in different electrolyte systems are presented in Fig. 26.

To the discussion of the PEO coating formation mechanism, it mainly combines the reactions between substrate material and electrolyte compounds, involving substrate oxidation and the deposition of species from the electrolyte [57]. Overall, the following reactions may occur during the PEO processing [41,55]:

$$Al \rightarrow Al^{3+} + 3e^- \tag{4}$$

$$2Al^{3+} + 3O^{2-} \rightarrow Al_2O_3 \tag{5}$$

$$2Al^{3+} + 6OH^- \rightarrow Al_2O_3 + 3H_2O \tag{6}$$

$$H_2O + SiO_3^{2-} \rightarrow SiO_2 + 2OH^- \tag{7}$$

$$SiO_2 + xAl_2O_3 \rightarrow SiO_2{\cdot}x(Al_2O_3) \tag{8}$$

where Eq. (4) represents the oxidation of substrate material, Eqs. (5) and (6) are responsible for the species from substrate in PEO layer formation and Eqs. (7) and (8) shows the role of silicates in the formation of PEO layer.

For OH- and P-based electrolytes, where coatings composed mainly from γ-Al_2O_3 and α-Al_2O_3, the substrate oxidation is the dominant reaction. Despite the same processing parameters, the morphology of the coatings is completely different, as mentioned above. The Eqs. (5) and (6) are the main processes for formation of PEO coatings for these systems with significant aluminium consumption with mainly inward growth mechanism. From the EDS analysis of the surface and cross-sections of the PEO layers, obtained in P-based electrolytes, only low content of P was detected (Table 2 and **Table SI-3**), while no detectable phosphate phase was seen during XRD measurements (Figs. 19–22). The reason can be that phosphates are complicated to deposit during the coatings formation or there are thermodynamic constraints on the stability of these phases. For example, it was shown earlier [37] that some phosphate containing phases (e.g. metaphosphate ($AlPO_4$) with a melting temperature of 1800 °C) can be formed on the coating/substrate interface. However, due to the instability of the phosphate phase in an alkaline solution, it cannot be seen during XRD measurements. For the PEO processing in Si-based electrolytes, both the deposition of SiO_3^{2-} species from the electrolyte and substrate oxidation simultaneously occur. Since, the deposition is stimulated by the discharges under high temperature (~7000 K) [58], more intense discharges with high energy lead to an intensive mixing of substrate and electrolyte components and rapid mullite formation (melting temperature of 1850 °C), according to the reactions (7) and (8).

Fig. 27 reveals a schematic diagram of PEO coating growth model in a ternary mixed OH-, Si- and P-based electrolytes. The formation of a PEO coating on Al is a complex process taking place under the cyclic action of melting (discharge) and quenching (electrolyte) due to the local high temperature and pressure. The growth of the ceramic coating occurs as it grows inward and outward the surface material, simultaneously [57,59]. It is believed, that at the beginning of the process, the coating grows mainly outwards. As the applied electrical potential increases with oxidation time due to the high heat-insulation properties of alumina layer, the molten aluminium as well as electrolyte components are oxidized and ejected through the discharge channels that are created by the breaking down of barrier oxide layer. The current, flowing in the places of breakdown, causes melting and evaporation of both the

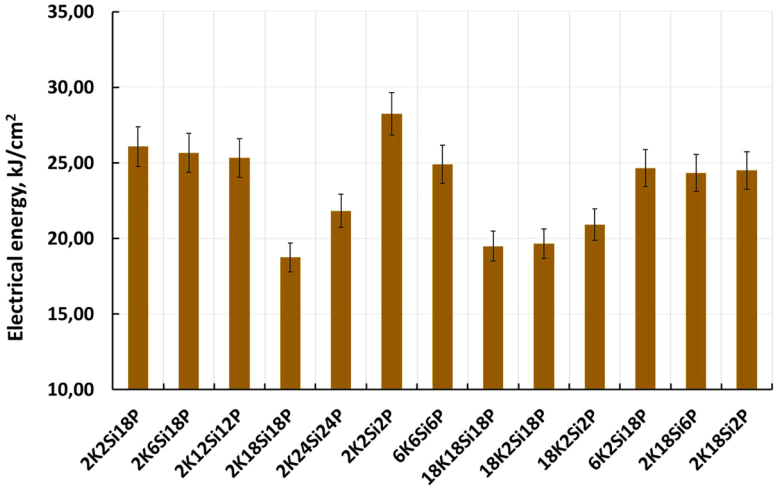

Fig. 25. The variation of the electrical energy for different PEO coatings.

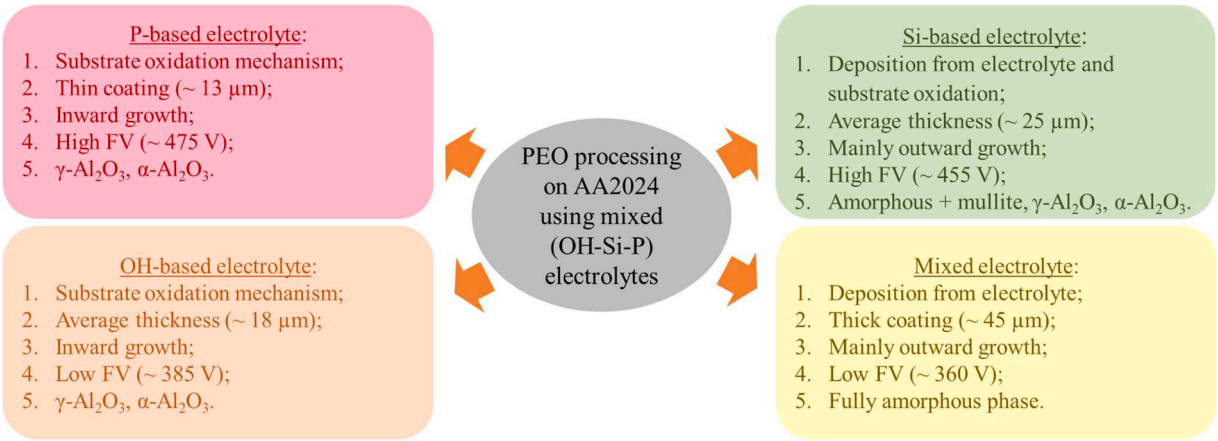

Fig. 26. Schematic illustration of PEO coatings characteristics obtained in different electrolytes.

substrate and the dielectric oxide layer. The molten material is rapidly solidified at the coating/electrolyte interface in a crater-like form. Then, with an increase of the treatment time, the outer layer of the coating becomes thicker, and the PEO layer predominantly grows inwards. At the same time, the coating continues to grow outwards. This phenomenon can be preferentially separated by changing the parameters of the PEO process, in particular, using different compositions of electrolytes.

The difference in the PEO coating thicknesses produced in OH-, P- and Si-based electrolytes can be associated with different coating formation behaviour, where coating growth is faster in Si-based electrolyte with predominantly outward growing mechanism (Fig. 27(**a**)). It is supposed that the different growth rate may originate from the effect of soluble anions (PO_4^{3-} and SiO_3^{2-}), especially due to their different adsorption characteristic, since the other process parameters were kept constant [59]. The SiO_3^{2-} anions from Si-based electrolytes enter into coating due to their stronger adsorptive actions. Due to high discharge energy resulting from high temperature and pressure during the process, the adsorption of dissolved anions on the coating surface takes place.

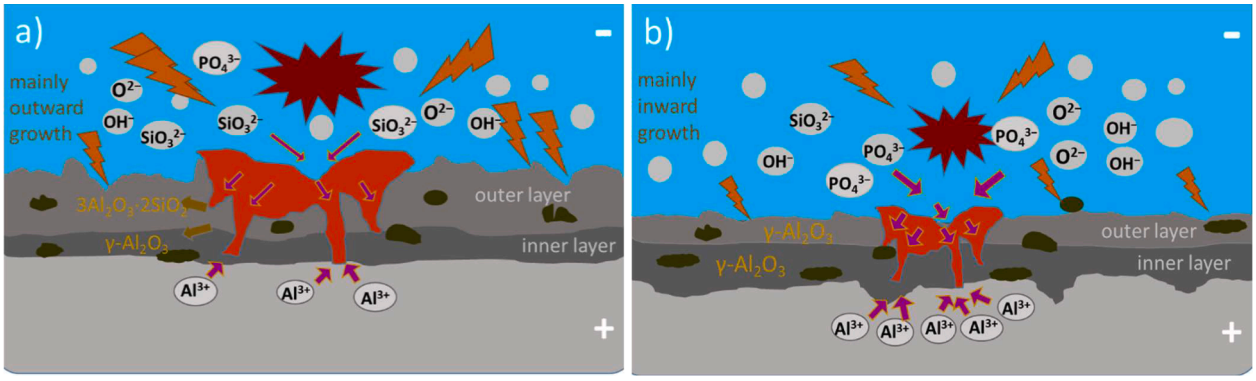

Fig. 27. Mechanism of PEO coating growth of Si-based electrolytes (a) and OH-, P-based electrolytes (b).

The rapid deposition of SiO_2 in the form of mullite under high temperatures can greatly improve coating growth rate in Si-based electrolyte, compared to PEO processing in phosphate-based electrolytes. The EDS analysis (Table 2) suggests that, deposition of silica is promoted in higher Si content electrolytes leading to enhanced thickening of the coatings, especially with amorphous structure. SEM cross-section maps (Figs. 10–13) reveals that the Si element is mainly distributed in the top layers of the coatings as well as around the pores and holes. It is suggested that due to a higher binding energy of SiO_2 species relative to that of the Al_2O_3 [58], the SiO_2 species mostly remain immobile in the outer region of the coatings. This mainly prevents diffusion of the substrate material to a coating surface, and the resulting coating grows mainly outwards.

For OH-, and P-based electrolytes (Fig. 27(**b**)), the increase of the coating is dominated by the inner growth of the layer during the PEO process as a result of the ejection of molten alumina through the discharge channels as well as oxygen diffusion. Thus, this would also be the reason for the low coating growth rate for respective specimens, since no other electrolyte components were involved in the process, based on XRD and EDS results. In addition, phosphates deposition on the coating/substrate interface can also be explained during PEO processing by the repeated secondary decomposition and solidification reactions, resulting in the cavities near the coating/substrate interface.

5. Conclusions

(1) The different composition ratios of the mixed alkaline electrolytes influence the morphology of PEO coatings on AA2024 alloy. For the coatings being produced in OH-based electrolyte, the surface reveals a huge porosity with large open pores. In P-based electrolyte more uniform coatings were obtained compared to Si electrolytes. The surface porosity not always correlate with internal porosity for PEO coatings obtained in mixed electrolytes.

(2) PEO coatings formed in OH- and P-based electrolytes are mainly composed of γ-Al_2O_3 crystalline phases. An amorphous phase in combination with mainly mullite crystalline phases is dominant in the coatings, produced in Si-based electrolytes and in the mixed electrolytes with higher concentrations of silicates (12–18 g/L).

(3) In mixed electrolytes (OH-Si-P) with low electrolyte concentrations (between 2 and 6 g/L), the crystalline structure of the coating is dominant; however, low coating growth rate is observed. For the PEO coatings, obtained in high concentrated mixed phosphate-silicate electrolytes (between 18 and 24 g/L), the presence of fully amorphous phase in the coating structure is observed together with high coating thickness.

(4) A relatively low coating growth rate, with dominating inward layer growth in OH-, and P-based electrolytes was observed. Si-based electrolytes contribute to preferential outward growth of the PEO coatings, where the deposition from the electrolyte and Al oxidation processes simultaneously occur. The thickening of the coatings mainly depends on the rapid deposition of bath compounds from Si-based electrolytes.

(5) A combination of low concentration of hydroxides, high concentration of phosphates with increasing concentration of silicates in the mixed electrolyte noticeably increases the coating thickness, improving also the uniformity and density of the coatings (e.g. 2K12Si12P, 2K24Si24P).

(6) On the one hand energy savings are mainly related to higher concentration electrolytes which on the other hand results in higher costs for the chemicals and disposal after use. However, higher coating growth rates in higher concentrated electrolytes may allow to shorten treatment times if a certain thickness is required. A proper analysis of costs and ecological impact of high concentrated electrolytes is quite complex and needs to be done for specific components/applications.

CRediT authorship contribution statement

G. Yeshmanova: Investigation, Visualization, Writing – original draft. **C. Blawert:** Conceptualization, Supervision, Writing – review & editing. **M. Serdechnova:** Visualization, Project administration, Writing – review & editing. **D.C. Florian Wieland:** Investigation, Writing – review & editing. **M. Starykevich:** Investigation, Writing – review & editing. **E. Gazenbiller:** Investigation, Writing – review & editing. **D. Höche:** Writing – review & editing. **D. Smagulov:** Supervision. **M.L. Zheludkevich:** Writing – review & editing.

Declaration of Competing Interest

The authors declare that they have no known competing financial interests or personal relationships that could have appeared to influence the work reported in this paper.

Data availability

Data will be made available on request.

Acknowledgments

The authors gratefully acknowledge PETRA III (Hamburg, Germany) for granting the P03 proposal I-20191340 for synchrotron X-ray diffraction analysis. The authors also thank Dr. Anton Davydok for the experimental support within those DESY beamline experiments. The technical support of Mr. Volker Heitmann, Mr. Ulrich Burmester and Mr. Gert Wiese during this work is gratefully appreciated. Partial financial support of this work was provided by REA Horizon 2020 research and innovation program in frame of Marie Sklodowska-Curie project FUNCOAT (823942).

Supplementary materials

Supplementary material associated with this article can be found, in the online version, at doi:10.1016/j.surfin.2023.103797.

References

[1] K. Babaei, A. Fattah-alhosseini, M. Molaei, The effects of carbon-based additives on corrosion and wear properties of Plasma electrolytic oxidation (PEO) coatings applied on Aluminum and its alloys: a review, Surf. Interfaces 21 (2020), 100677.
[2] M. Aliofkhazraei, D.D. Macdonald, E. Matykina, E.V. Parfenov, V.S. Egorkin, J. A. Curran, S.C. Troughton, S.L. Sinebryukhov, S.V. Gnedenkov, T. Lampke, F. Simchen, H.F. Nabavi, Review of plasma electrolytic oxidation of titanium substrates: mechanism, properties, applications and limitations, Appl. Surf. Sci. Adv. 5 (2021), 100121.
[3] A. Fattah-alhosseini, R. Chaharmahali, K. Babaei, Effect of particles addition to solution of plasma electrolytic oxidation (PEO) on the properties of PEO coatings formed on magnesium and its alloys: a review, J. Magnes. Alloy. 8 (3) (2020) 799–818.
[4] G.B. Darband, M. Aliofkhazraei, P. Hamghalam, N. Valizade, Plasma electrolytic oxidation of magnesium and its alloys: mechanism, properties and applications, J. Magnes. Alloy. 5 (1) (2017) 74–132.
[5] W. Yao, L. Wu, J. Wang, B. Jiang, D. Zhang, M. Serdechnova, T. Shulha, C. Blawert, M.L. Zheludkevich, F. Pan, Micro-arc oxidation of magnesium alloys: a review, J. Mater. Sci. Technol. (10) (2022) 158–180.
[6] Y. Li, D. Zhang, C. Qi, Y. Xue, Y. Wan, H. Sun, Enhanced corrosion and tribocorrosion behavior of plasma electrolytic oxidized coatings on 5052 aluminum alloy with addition of pullulan to silicate electrolyte, J. Alloy. Compd. 960 (2023), 170782.
[7] L.Y. An, Y. Ma, X.X. Yan, Sh. Wang, Z.Y. Wang, Effects of electrical parameters and their interactions on plasma electrolytic oxidation coatings on aluminum substrates, Trans. Nonferrous Met. Soc. China 30 (2020) 883–895.
[8] M. Sieber, F. Simchen, R. Morgenstern, I. Scharf, T. Lampke, Plasma electrolytic oxidation of high-strength aluminium alloys—substrate effect on wear and corrosion performance, Metals 5 (2018) 356.
[9] W. Liu, Y. Liu, Y. Lin, Z. Zhang, Sh. Feng, M. Talha, Y. Shi, T. Shi, Effects of graphene on structure and corrosion resistance of plasma electrolytic oxidation coatings formed on D16T Al alloy, Appl. Surf. Sci. 475 (2019) 645–659.

[10] B. Yin, Z. Peng, J. Liang, K. Jin, S. Zhu, J. Yang, Z. Qiao, Tribological behavior and mechanism of self-lubricating wear-resistant composite coatings fabricated by one-step plasma electrolytic oxidation, Tribol. Int. 97 (2016) 97–107.
[11] T. Wu, C. Blawert, M. Serdechnova, P. Karlova, G. Dovzhenko, D.C.F. Wieland, S. Stojadinovic, R. Vasilic, L. Wang, C. Wang, K. Mojsilovic, M.L. Zheludkevich, Role of phosphate, silicate and aluminate in the electrolytes on PEO coating formation and properties of coated Ti6Al4V alloy, Appl. Surf. Sci. 595 (2022), 153523.
[12] S. Sela, K. Borodianskiy, Synthesis of ceramic surface on Zr alloy using plasma electrolytic oxidation in molten salt, Surf. Interfaces 36 (2023), 102533.
[13] A. Sobolev, D. Bograchev, M. Zinigrad, K. Borodianskiy, Evolution of corrosion on microstructure of ceramic coating produced by plasma electrolytic oxidation in molten salt, Ceram. Int. 48 (8) (2022) 10990–10998.
[14] L. Zhu, X. Ke, J. Li, Y. Zhang, Z. Chen, Z. Zhang, Y. Lu, M. Sui, Growth mechanisms for initial stages of plasma electrolytic oxidation coating on Al, Surf. Interfaces 25 (2021), 101186.
[15] W.Y. Liu, Y. Liu, C. Blawert, M.L. Zheludkevich, Ch.L. Fan, M. Talha, Y.H. Lin, Microstructure, wear and corrosion performance of plasma electrolytic oxidation coatings formed on D16T Al alloy, Rare Met. 39 (12) (2020) 1425–1439.
[16] J.H. Lee, K.H. Jung, S.J. Kim, Characterization of ceramic oxide coatings prepared by plasma electrolytic oxidation using pulsed direct current with different duty ratio and frequency, Appl. Surf. Sci. 516 (2020), 146049.
[17] G. Lv, W. Gu, H. Chen, W. Feng, M.L. Khosa, L. Li, E. Niu, G. Zhang, S.Z. Yang, Characteristic of ceramic coatings on aluminum by plasma electrolytic oxidation in silicate and phosphate electrolyte, Appl. Surf. Sci. 253 (2006) 2947–2952.
[18] Ch. Yang, J. Zhu, S. Cui, P. Chen, Z. Wu, Z. Ma, R.K.Y. Fu, X. Tian, P.K. Chu, Zh. Wu, Wear and corrosion resistant coatings prepared on LY12 aluminum alloy by plasma electrolytic oxidation, Surf. Coat. Technol. 409 (2021), 126885.
[19] H.J. Xie, Y.L. Cheng, S.X. Li, J.H. Cao, L. Cao, Wear and corrosion resistant coatings on surface of cast A356 aluminum alloy by plasma electrolytic oxidation in moderately concentrated aluminate electrolytes, Trans. Nonferrous Met. Soc. China 27 (2017) 336–351.
[20] W.C. Gu, G.H. Lv, H. Chen, G.L. Chen, W.R. Feng, G.L. Zhang, S.Z. Yang, Investigation of morphology and composition of plasma electrolytic oxidation coatings in systems of Na_2SiO_3–NaOH and $(NaPO_3)_6$–NaOH, J. Mater. Process. Technol. 182 (1–3) (2007) 28–33.
[21] E. Matykina, R. Arrabal, M. Mohedano, B. Mingo, J. Gonzalez, A. Pardo, M. C. Merino, Recent advances in energy efficient PEO processing of aluminium alloys, Trans. Nonferrous Met. Soc. China 27 (2017) 1439–1454.
[22] S.H. Deng, D.Q. Yi, Z.Q. Gong, Y.C. Su, Influence of potential on the structure and properties of microarc oxidation coating on Mg alloy, Anti Corros. Methods Mater. 55 (5) (2008) 264–269.
[23] F. Jaspard-Mécuson, T. Czerwiec, G. Henrion, T. Belmonte, L. Dujardin, A. Viola, J. Beauvir, Tailored aluminium oxide layers by bipolar current adjustment in the plasma electrolytic oxidation (PEO) process, Surf. Coat. Technol. 201 (2007) 8677–8682.
[24] A. Hakimizad, K. Raeissi, M. Santamaria, M. Asghari, Effects of pulse current mode on plasma electrolytic oxidation of 7075 Al in Na_2WO_4 containing solution: from unipolar to soft-sparking regime, Electrochim. Acta 284 (2018) 618–629.
[25] S. Ignjatović, C. Blawert, M. Serdechnova, S. Karpushenkov, M. Damjanović, P. Karlova, G. Dovzhenko, D.C.F. Wieland, B. Zeller-Plumhoff, M. Starykevich, S. Stojanović, L. Damjanović-Vasilić, M.L. Zheludkevich, The influence of *in situ* anatase particle addition on the formation and properties of multifunctional plasma electrolytic oxidation coatings on AA2024 aluminum alloy, Adv. Eng. Mater. 23 (2021), 2001527.
[26] A.C. Bouali, E.A. Straumal, M. Serdechnova, D.C.F. Wieland, M. Starykevich, C. Blawert, J.U. Hammel, S.A. Lermontov, M.G.S. Ferreira, M.L. Zheludkevich, Layered double hydroxide based active corrosion protective sealing of plasma electrolytic oxidation/sol-gel composite coating on AA2024, Appl. Surf. Sci. 494 (2019) 829–840.
[27] M. Mohedano, B. Mingo, H. Mora-Sánchez, E. Matykina, R. Arrabal, Effects of pre-anodizing and phosphates on energy consumption and corrosion performance of PEO coatings on AA6082, Surf. Coat. Technol. 409 (2021), 126892.
[28] M. Serdechnova, S.A. Karpushenkov, L.S. Karpushenkava, M. Starykevich, M.G. S. Ferreira, T. Hack, M.H. Iuzviuk, I.A. Zobkalo, C. Blawert, M.L. Zheludkevich, The influence of PSA pre-anodization of AA2024 on PEO coating formation: composition, microstructure, corrosion, and wear behaviors, Materials 11 (2018) 2428.
[29] M. Tang, W. Li, H. Liu, L. Zhu, Preparation Al_2O_3/ZrO_2 composite coating in an alkaline phosphate electrolyte containing K_2ZrF_6 on aluminum alloy by microarc oxidation, Appl. Surf. Sci. 258 (2012) 5869–5875.
[30] E. Erfanifar, M. Aliofkhazraei, H. Fakhr Nabavi, H. Sharifi, A.S. Rouhaghdam, Growth kinetics and morphology of plasma electrolytic oxidation coating on aluminum, Mater. Chem. Phys. 185 (2017) 162–175.
[31] Y. Mori, A. Koshi, J. Liao, H. Asoh, S. Ono, Characteristics and corrosion resistance of plasma electrolytic oxidation coatings on AZ31B Mg alloy formed in phosphate – Silicate mixture electrolytes, Corros. Sci. 88 (2014) 254–262.
[32] Y.K. Wu, Z. Yang, R.Q. Wang, G.R. Wu, D. Chen, D.D. Wang, X.T. Liu, D.L. Li, C. H. Guo, S.X. Yu, D.J. Shen, P. Nash, An investigation of microstructure evolution for plasma electrolytic oxidation (PEO) coated Al in an alkaline silicate electrolyte, Surf. Coat. Technol. 351 (2018) 136–152.
[33] L. Pezzato, D. Vranescu, M. Sinico, C. Gennari, A.G. Settimi, P. Pranovi, K. Brunelli, M. Dabalà, Tribocorrosion properties of PEO coatings produced on AZ91 magnesium alloy with silicate- or phosphate-based electrolytes, Coatings 8 (2018) 202.
[34] A. Fattah-Alhosseini, M. Vakili-Azghandi, M.K. Keshavarz, Influence of concentrations of KOH and Na_2SiO_3 electrolytes on the electrochemical behavior of ceramic coatings on 6061 Al alloy processed by plasma electrolytic oxidation, Acta Metall. Sin. 29 (3) (2016) 274–281 (English Letters).
[35] A. Polat, M. Makaraci, M. Usta, Influence of sodium silicate concentration on structural and tribological properties of microarc oxidation coatings on 2017A aluminum alloy substrate, J. Alloy. Compd. 504 (2010) 519–526.
[36] C. Jiang, Y. Wang, Sh. Wang, Y. Zou, J. Ouyang, D. Jia, Y. Zhou, Growth characteristics and properties of plasma electrolytic oxidation coatings produced in different electrolytes on SiCp/Al composite, Mater. Charact. 205 (2023), 113344.
[37] Sh. Wang, X. Liu, X. Yin, N. Du, Influence of electrolyte components on the microstructure and growth mechanism of plasma electrolytic oxidation coatings on 1060 aluminum alloy, Surf. Coat. Technol. 381 (2020), 125214.
[38] A. Freddy, C. Barbante, History and present status of micro- and nano-imaging analysis, Compr. Anal. Chem. 69 (2015) 67–124 [Chemical Imaging Analysis].
[39] C. Krywka, H. Neubauer, M. Priebe, T. Salditt, J. Keckes, A. Buffet, S.V. Roth, R. Doehrmann, M. Mueller, A two-dimensional waveguide beam for X-ray nanodiffraction, J. Appl. Crystallogr. 45 (2012) 85–92.
[40] G. Ashiotis, A. Deschildre, Z. Nawaz, J.P. Wright, D. Karkoulis, F.E. Picca, J. Kieffer, The fast azimuthal integration Python library: pyFAI, J. Appl. Crystallogr. 48 (2) (2015) 510–519.
[41] A. Fattah-Alhosseini, S.O. Gashti, M. Molaie, Effects of disodium phosphate concentration ($Na_2HPO_4{\cdot}2H_2O$) on microstructure and corrosion resistance of plasma electrolytic oxidation (PEO) coatings on 2024 Al alloy, J. Mater. Eng. Perform. 27 (2018) 825–834.
[42] X. Yang, L. Chen, Y. Qu, R. Liu, K. Wei, W. Xue, Optical emission spectroscopy of plasma electrolytic oxidation process on 7075 aluminum alloy, Surf. Coat. Technol. 324 (2017) 18–25.
[43] V. Bordo, T. Ebel, First-principles theory of electrical breakdown in barrier anodic films in contact with an electrolyte, Electrochim. Acta 354 (2020), 136490.
[44] A. Seyfoori, Sh. Mirdamadi, A. Khavandi, Z. Seyed Raufi, Biodegradation behavior of micro-arc oxidized AZ31 magnesium alloys formed in two different electrolytes, Appl. Surf. Sci. 261 (2012) 92–100.
[45] F. Di Quarto, S. Piazza, C. Sunseri, Electrical and mechanical breakdown of anodic films on tungsten in aqueous electrolytes, J. Electroanal. Chem. 248 (1988) 99–115.
[46] G.E. Thompson, Y. Xu, P. Skeldon, K. Shimizu, S.H. Han, G.C. Wood, Anodic oxidation of aluminium, Philos. Mag. Part B 55 (1987) 651–667.
[47] J. Martin, A. Nominé, V. Ntomprougkidis, S. Migot, S. Bruyère, F. Soldera, T. Belmonte, G. Henrion, Formation of a metastable nanostructured mullite during Plasma Electrolytic Oxidation of aluminium in “soft” regime condition, Mater. Des. 180 (2019), 107977.
[48] D.D. Wang, X.T. Liu, Y.K. Wu, H.P. Han, Z. Yang, Y. Su, X.Z. Zhang, G.R. Wu, D. J. Shen, Evolution process of the plasma electrolytic oxidation (PEO) coating formed on aluminum in an alkaline sodium hexametaphosphate ($(NaPO_3)_6$) electrolyte, J. Alloy. Compd. 798 (2019) 129–143.
[49] R. Liu, J. Wu, W. Xue, Y. Qu, C. Yang, B. Wang, X. Wu, Discharge behaviors during plasma electrolytic oxidation on aluminum alloy, Mater. Chem. Phys. 148 (2014) 284–292.
[50] R.O. Hussein, X. Nie, D.O. Northwood, A. Yerokhin, A. Matthews, Spectroscopic study of electrolytic plasma and discharging behaviour during the plasma electrolytic oxidation (PEO) process, J. Phys. D: Appl. Phys. 43 (2010), 105203.
[51] F. Liu, J.L. Xu, D.Z. Yu, F.P. Wang, L.C. Zhao, Effects of cathodic voltages on the structure and properties of ceramic coatings formed on NiTi alloy by micro-arc oxidation, Mater. Chem. Phys. 121 (2010) 172–177.
[52] R.O. Hussein, P. Zhang, X. Nie, Y. Xia, D.O. Northwood, The effect of current mode and discharge type on the corrosion resistance of plasma electrolytic oxidation (PEO) coated magnesium alloy AJ62, Surf. Coat. Technol. 206 (2011) 1990–1997.
[53] A.L. Yerokhin, X. Nie, A. Leyland, A. Matthews, S.J. Dowey, Plasma electrolysis for surface engineering, Surf. Coat. Technol. 122 (1999) 73–93.
[54] J.H. Lee, S.J. Kim, Effects of silicate ion concentration on the formation of ceramic oxide layers produced by plasma electrolytic oxidation on Al alloy, Jpn. J. Appl. Phys. 56 (2017) 01AB01.
[55] X. Liu, S. Wang, N. Du, X. Li, Q. Zhao, Evolution of the three-dimensional structure and growth model of plasma electrolytic oxidation coatings on 1060 aluminum alloy, Coatings 8 (2018) 105.
[56] M. Mohedano, E. Lopez, B. Mingo, S. Moon, E. Matykina, R. Arrabal, Energy consumption, wear and corrosion of PEO coatings on preanodized Al alloy: the influence of current and frequency, J. Mater. Res. Technol. 21 (2022) 2061–2075.
[57] Q. Li, C.C. Liu, W.B. Yang, J. Liang, Growth mechanism and adhesion of PEO coatings on 2024Al alloy, Surf. Eng. 33 (2016) 760–766.
[58] F. Monfort, A. Berkani, E. Matykina, P. Skeldon, G.E. Thompson, H. Habazaki, K. Shimizu, Development of anodic coatings on aluminium under sparking conditions in silicate electrolyte, Corros. Sci. 49 (2007) 672–693.
[59] J. Li, H. Cai, X. Xue, B. Jiang, The outward–inward growth behavior of microarc oxidation coatings in phosphate and silicate solution, Mater. Lett. 64 (2010) 2102–2104.